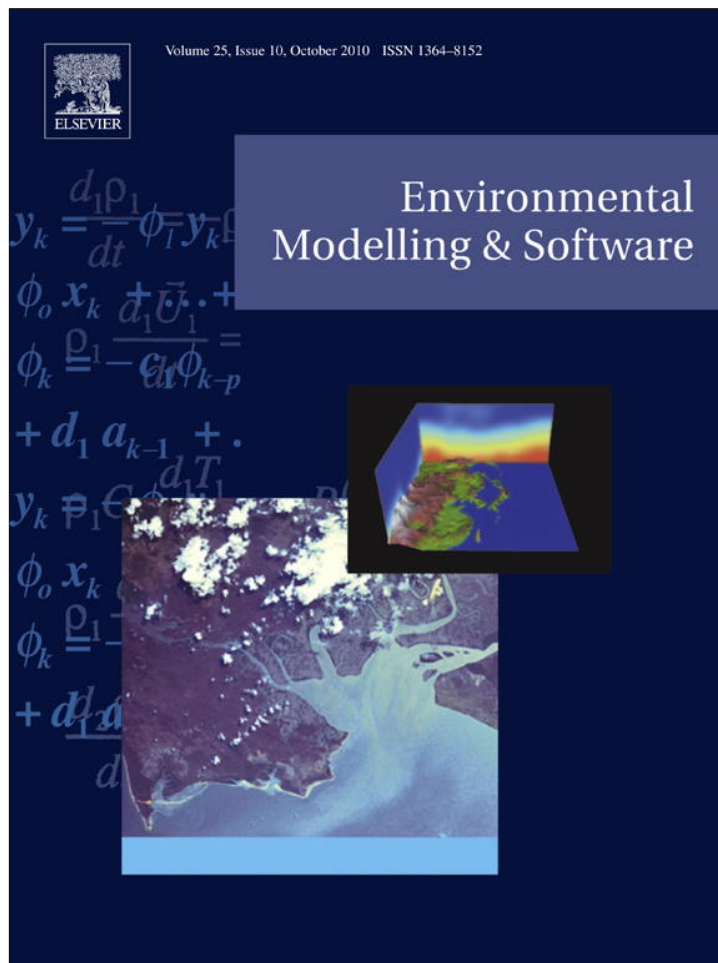


Provided for non-commercial research and education use.  
Not for reproduction, distribution or commercial use.



This article appeared in a journal published by Elsevier. The attached copy is furnished to the author for internal non-commercial research and education use, including for instruction at the authors institution and sharing with colleagues.

Other uses, including reproduction and distribution, or selling or licensing copies, or posting to personal, institutional or third party websites are prohibited.

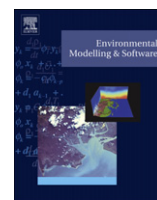
In most cases authors are permitted to post their version of the article (e.g. in Word or Tex form) to their personal website or institutional repository. Authors requiring further information regarding Elsevier's archiving and manuscript policies are encouraged to visit:

<http://www.elsevier.com/copyright>



Contents lists available at ScienceDirect

## Environmental Modelling &amp; Software

journal homepage: [www.elsevier.com/locate/envsoft](http://www.elsevier.com/locate/envsoft)

# Wind characteristics over complex terrain with implications for bushfire risk management

J.J. Sharples<sup>a,b,\*</sup>, R.H.D. McRae<sup>b,c</sup>, R.O. Weber<sup>a,b</sup>

<sup>a</sup> School of Physical, Environmental and Mathematical Sciences, University of New South Wales at the Australian Defence Force Academy, Canberra, ACT 2600, Australia

<sup>b</sup> Bushfire Cooperative Research Centre, Level 5, 340 Albert St. East Melbourne, VIC 3002, Australia

<sup>c</sup> ACT Emergency Services Agency, Curtin, ACT 2605, Australia

## ARTICLE INFO

### Article history:

Received 29 April 2009

Received in revised form

Accepted 16 March 2010

### Keywords:

Wind

Topography

Wind-terrain interaction

Joint distribution

Bushfire

Fire spread modelling

Bushfire risk modelling

## ABSTRACT

Understanding spatially distributed wind fields over complex terrain is important for a variety of applications including pollutant dispersion modelling, fire spread modelling and bushfire risk management. Directional changes in surface winds are particularly important in the context of fire management. In this paper terrain-modified winds are analysed using joint probability distributions derived from wind speed and direction data collected in rugged terrain to the west and southwest of the Australian Capital Territory. The analyses focus on two landform elements; a steep slope and a moderately steep valley. The joint distributions prove to be useful tools for identifying and characterising the dominant states of the wind-terrain systems. Several processes, including thermally-driven winds, lee-slope eddies and dynamic channelling are identified and discussed. The analyses also reveal the stochastic nature of the wind-terrain systems, and thus raise some doubts about the suitability of some deterministic approaches used to model terrain-modified surface winds. Implications of the results relevant to fire behaviour and bushfire risk management are also discussed.

© 2010 Elsevier Ltd. All rights reserved.

## 1. Introduction

It is well known that complex or rugged terrain can have a significant effect on micro- and meso-scale atmospheric flows (Blumen, 1990; Barry, 1992; Whiteman, 2000). As a consequence, surface wind fields in rugged terrain can be highly variable, both across space and in time. Understanding these dynamic wind fields is an important part of many environmental problems, for example, the atmospheric dispersion of pollutants, aerial spraying and the prediction of how a wildfire will spread (Kossmann et al., 2001). Terrain-induced flows are also important considerations for light aviation and generally affect the local climatology of mountainous regions. In this paper the focus will be on these dynamic wind fields in the context of wildfire or bushfire risk modelling, which generally includes some form of fire spread modelling (Chandler et al., 1983; Beer, 1991).

Fire spread models permit those concerned with fire management to estimate how a fire will spread under certain conditions, thereby facilitating the better deployment of resources during fire

suppression activities, and more targeted fuel reduction treatments as part of longer term fire management practices. Typically fire spread models require information on the amount and type of combustible fuel, drought conditions, topography and meteorological variables such as wind speed and direction, temperature and relative humidity. In particular, fire spread models are highly sensitive to changes in wind direction.

To accurately simulate the spread of a fire, it is therefore desirable to use wind speed and direction data that matches the actual conditions on a fire-ground as closely as possible. However, given the difficulty of predicting surface wind fields in general, common practice has been to simply extrapolate wind direction data from the closest source of meteorological information, which can sometimes be tens of kilometres away. In the most simple of these approaches wind speed and direction are assumed constant over the entire fire-ground. While this assumption may be appropriate over flat or gently undulating terrain, applying such a simplistic approach in rugged terrain can lead to serious errors in assessing the likely spread of a fire. Specifically, the assumption of constant wind speed and direction fails to recognise the nonlinear or turbulent effects that the terrain can have on local winds. Examples of such effects include eddy winds, thermally-driven winds and dynamic channelling (Lee et al., 1981; Wippermann and Gross, 1981; Wippermann, 1984; Doran and Whiteman, 1992; Eckman et al., 1992; Whiteman and

\* Corresponding author. School of Physical, Environmental and Mathematical Sciences, University of New South Wales at the Australian Defence Force Academy, Canberra, ACT 2600, Australia. Tel.: +61 2 6268 9466; fax: +61 2 6268 8786.  
E-mail address: [j.sharples@adfa.edu.au](mailto:j.sharples@adfa.edu.au) (J.J. Sharples).

Doran, 1993; Weber and Kauffmann, 1998; Kossman and Sturman, 2002, 2003). Thermally-driven winds can dominate surface wind patterns when ambient winds are light (McCutchan, 1983; McCutchan and Fox, 1986; Sturman, 1987; Whiteman, 1990, 2000) while eddy winds and dynamic channelling, in particular, have been identified as efficient mechanisms for the development of large fires in rugged terrain (Byron-Scott, 1990; Whiteman, 2000; Kossman et al., 2001).

Dynamic channelling occurs through the interaction of the ambient winds with certain terrain features. Incised valleys and gaps between mountains can have winds channelled along or between them in response to local differences in friction or pressure (Whiteman and Doran, 1993; Kossman et al., 2001). Forced channelling results when the valley side-walls cause frictional differences which are much less in the along-valley direction than they are in the across-valley direction. This frictional difference forces the wind to align preferentially along the valley axis, with the strength and direction of the channelled flow dependent upon the sign and magnitude of the component of the ambient winds relative to the valley axis (Doran and Whiteman, 1992; Whiteman and Doran, 1993; Kossman et al., 2001; Kossman and Sturman, 2002). Pressure-driven channelling occurs when the air within a valley responds to the component of the geostrophic pressure gradient along the valley axis (Fiedler, 1983). Pressure driven channelling is mainly responsible for modification of large scale winds in broad and long valleys (Wippermann and Gross, 1981; Whiteman and Doran, 1993), whereas forced channelling mainly occurs in smaller valleys, mountain passes or saddles (Weber and Kauffmann, 1998). A study by Smedman et al. (1996) on intermediate valleys suggests that both pressure-driven and forced channelling processes can occur in combination.

Eddy winds result as a consequence of the separation of the ambient flow from the terrain surface. Lee-slope eddies, in particular, often form on steep lee-slopes of mountain ridges or isolated hills (Whiteman, 2000). In general, the characteristics of the airflow in the lee of topography are dependent upon the steepness and roughness of the terrain, the speed of the ambient winds and the stability of the atmosphere (Scorer, 1955; Jackson and Hunt, 1975; Mason and Sykes, 1979; Hunt and Snyder, 1980; Tampieri, 1987; Taylor et al., 1987; Wood and Mason, 1993; Wood, 1995, 2000; Bowen, 2003; Lewis et al., 2008). For example, at a sharp edge at the top of a ridge, separation will occur very readily under most conditions, while for more rounded terrain profiles separation of the flow will depend on conditions of stability and the ambient wind speed as described by the Froude number:

$$F = \frac{U}{\sqrt{hS}}$$

where  $U$  is the ambient wind speed,  $h$  is the mountain height and  $S$  is the static stability (Barry, 1992). Flow separation on lee-slopes is favoured when  $F$  is greater than unity and so is more likely to occur under neutral or unstable conditions when ambient winds are strong (Barry, 1992; Wood, 1995; Whiteman, 2000). Wood (1995) reports that for a neutral, turbulent flow, separation will generally occur when the lee-slope exceeds a critical value of approximately  $20^\circ$ . This is consistent with Grant and Mason (1990) who advise that it may be reasonable to assume flow separation for topography with maximum slopes greater than  $15^\circ$ – $20^\circ$ .

In essence, the effects described above can all result in directional changes in the local wind field, which can then differ from the ambient wind direction by up to  $90^\circ$ , in the case of forced channelling, or  $180^\circ$  in the case of pressure-driven channelling and eddy and thermally-driven winds. Unexpected wind changes of such magnitudes can seriously compromise fire suppression activities and

fire-crew safety. Understanding the intricacies of rugged terrain-wind systems is therefore an important part of understanding the associated fire regime and can improve the safety and effectiveness of fire management strategies (Sharples, 2009).

To address the problem of accurately modelling fire spread in rugged terrain, more sophisticated fire spread models incorporate components designed to make local modifications to surface winds based on topographic considerations. A number of methods have been employed. Examples include computational fluid dynamics (CFD) methods, which simulate the surface wind field by numerically solving the fluid equations with the terrain surface as a boundary for the problem (Alm and Nygaard, 1995; Kim and Boysan, 1999; Kim et al., 2000; Lopes, 2003; Forthofer et al., 2003; Butler et al., 2006a, 2006b; Forthofer and Butler, 2007; Forthofer, 2007), mass continuity or kinematic methods, which simulate surface wind fields using the equations of conservation of mass along with the terrain surface as a boundary for the problem (Sherman, 1978; Davis et al., 1984; Moussiopoulos and Flassak, 1986; Ross et al., 1988; Forthofer, 2007) and methods that modify the surface wind field using a table of correction factors that depend on topographic aspect and ambient wind direction, or other simple rules of thumb (e.g. McRae, 1997). Mesoscale numerical weather prediction models have also been used to simulate the terrain-modified flow and have even been coupled with fire spread models (Linn, 1997; Coen, 2005; Winterkamp et al., 2006; Linn et al., 2007).

Modelling surface wind fields using CFD methods or numerical weather models can produce accurate information on surface wind fields but has the disadvantage of being computationally intensive, requiring resources that may not be available to the average fire management agency. Kinematic methods have the disadvantage of not accurately reproducing changes in wind direction caused by turbulent and thermal effects. Likewise, the simplistic nature of methods employing tables or rules of thumb can fail to capture directional changes due to nonlinear and thermal effects.

In this paper we discuss an empirical approach to understanding the directional component of a particular wind-terrain system, based on probabilistic analyses of wind direction data collected by the authors. It is important to note that while terrain effects on wind speed and turbulence intensity are also extremely important for the propagation of bushfires, our focus here is on the directional aspect of wind. The approach focuses on joint wind direction distributions for a number of different paired locations, and is an extension of an approach used by Whiteman and Doran (1993) to analyse the relationship between synoptic-scale winds and winds in a mesoscale valley.

We concentrate on rugged landforms within the Brindabella and Tidbinbilla Ranges to the west and southwest of Canberra, ACT. The general synoptic pattern during summer over the region is dominated by the passage of high-pressure systems that produce west-northwesterly winds. During winter the high-pressure ridge tracks along a more southerly route producing more westerly winds.

We begin in section 2 by outlining the methods employed in the field-data collection and describing the locations and characteristics of the individual sites used in the study. Section 3 discusses the analytical methods used to construct the joint wind direction distributions, before they are analysed in section 4. The results of section 4 are further discussed, in the context of bushfire risk management, in section 5. Although the study presented here is primarily motivated by an application in bushfire risk management and aimed at the fire meteorology community, it is also relevant to the broader mountain meteorological community. Indeed, the presentation and discussion of the data would be of great relevance to light and recreational aviation and to pollution dispersion problems, in addition to researchers interested in the development and validation of computational wind models.

## 2. Field-data collection methods

The existing national network of automatic weather stations, maintained by the Bureau of Meteorology, is not dense enough to investigate the micro- and meso-scale phenomena of interest in the fire management context. For this reason additional portable automatic weather stations were deployed in close proximity (with an average spacing of the order of 100–1000 m) in the area of interest. Augmenting the Bureau's network in this way enables the capture of finer-scale phenomena in addition to the broader scale meteorology. Specifically we used Davis Vantage Pro2™ weather stations with WeatherLink® data loggers. The Vantage Pro2™ includes an integrated sensor suite with temperature and humidity sensors and a wind vane and cup anemometer.

Field-data collection concentrated on two regions to the west and southwest of Canberra, ACT. In particular, we deployed portable automatic weather stations in Tidbinbilla Nature Reserve, ACT and Brindabella National Park, NSW, which form part of the mountainous region to the west of the Australian Capital Territory. These particular areas were chosen because they both contained complex topography and had both experienced severe fire behaviour during the January 2003 alpine fires (Nairn, 2003; McRae, 2004; McRae et al., 2006; Mills, 2006), which had removed a lot of the natural forest canopy. In addition, both areas had reasonable access, but were still secluded enough so that the risk of people tampering with the deployed instrumentation was minimal. Concentrating on these areas also meant that the wind data being collected could assist in understanding the intense fire behaviour observed in them.

The wind vanes and anemometers were mounted on masts at a height of 5 m above the ground surface. The standard height at which wind is measured in Australia is 10 m. However, experience has shown that wind measurements at a height of 5 m, particularly those pertaining to wind direction in sparse canopy, do not differ significantly from those at 10 m (Holtslag, 1984; Van Ulden and Holtslag, 1985). Given this, and the logistics of field deployment, it was decided that measurement of wind at 5 m would be sufficient. The integrated sensor suites were fixed to masts at a height of 2 m, while solar panels to power the stations were fitted to the mast at a height of 1 m. In total, eleven portable automatic weather stations were deployed in the field.

The stations were deployed on two main landform elements. In Tidbinbilla Nature Reserve, stations were deployed along the ridge and on the east-facing slopes of a steep mountain ridge (known as 'Camel's Back') with a relief of approximately 500 m. In Brindabella National Park stations were deployed across a mountain valley (Flea Creek) with reasonably steep slopes and a relief of approximately 300–400 m. Both the mountain ridge and the valley are aligned roughly in a north–south direction. Where possible the stations were deployed at sites with very little or no canopy so that we could minimise the effects of the canopy on the wind data being recorded. Given the realities of the field setting, however, this was not always entirely possible (see Table 1). In total, three transects of portable automatic weather stations were deployed: two in Tidbinbilla Nature Reserve, one running northwest to southeast and one running southwest to northeast, and one in Brindabella National Park running roughly west to east.

The three transects were defined by three ridge-top locations and were comprised of an approximately linear array of weather stations. We say 'approximately linear' since the difficulties of the terrain prevented us from aligning the stations perfectly. The two transects at Tidbinbilla will be denoted A and B, and the Brindabella transect will be denoted C. Transect A consists of the four locations A1, A2, A3 and A4, transect B consists of the four locations B1, B2, B3 and B4, while transect C consists of the five

locations C1, C2, C3, C4 and C5. The positions and descriptions of the thirteen locations referred to above are given in Table 1. Note that A4 and B4 both indicate the same location, which has been utilised in both transects A and B. A map showing the locations and the underlying topography can be seen in Fig. 1. We also use data from two Bureau of Meteorology automatic weather stations not listed in Table 1. The two stations are at Canberra Airport (CA, 149.20°E, 35.30°S, 578 m ASL) and Mt Ginini (MG, 148.77°E, 35.53°S, 1760 m ASL).

The deployed automatic weather stations were initially programmed to record data at 30 min intervals, however, accessing the stations to download the recorded data, became more problematic and dangerous during the winter months due to the presence of ice and snow on the steep slopes. It was therefore decided that a sampling time of 1 h would be used over the winter months to extend the time between successive visits to download the data. Wind directions were given in terms of the sixteen standard points of the compass rose: N, NNE, NE, etc. Recorded wind directions were the dominant (modal) wind directions over the sampling interval, while recorded wind speeds were the means of the sampled wind speeds. Wind speed and direction were sampled every 15 s when the sampling interval was 30 min, and every 30 s when the sampling interval was 1 h.

## 3. Method of analysis

In the analyses we consider data from selected pairs of stations across the landscape. The first of the two stations will be taken to be indicative of the ambient wind direction, while the second is indicative of the wind direction pattern at some nearby location within the landscape. In what follows we will take the first station to be a ridge-top station, while the second station will be located on a nearby slope, for example. In the terminology associated with CFD methods, for example, the wind directions at the first and second stations could be construed as input and response, respectively. We denote the wind direction experienced at the first station by  $\theta_1$  and the wind direction at the second station by  $\theta_2$ , where  $0^\circ \leq \theta_1, \theta_2 \leq 360^\circ$ .

The ordered pair  $\mathbf{p} = (\theta_1, \theta_2)$  can be thought of as a state variable for the joint wind direction system for the two station locations. To gain an understanding of the stochastic nature of the joint wind direction system for the two locations in question, it is natural to consider the joint wind direction distribution for the two stations. To construct the joint wind direction distribution we took data from the pair of stations and matched wind direction records according to date and time. We denote the set of matched pairs as  $P$ , and suppose that  $P$  contains  $M$  pairs of wind direction data. That is,

$$P = \left\{ \mathbf{p}^i = (\theta_1^i, \theta_2^i) : i = 1, \dots, M \right\}.$$

Throughout this paper we will use the compass points N, NNE, NE, etc. interchangeably with their corresponding values in degrees  $0^\circ, 22.5^\circ, 45^\circ$ , etc. Hence, the pair (WNW, SE) is the same as  $(292.5^\circ, 135.0^\circ)$ .

Since the sampled wind direction data is given in terms of the sixteen standard compass points, it is natural to consider the  $17 \times 17$  grid whose lower left vertices are given by the vectors  $\mathbf{x}_{jk} = (22.5^\circ(j-1), 22.5^\circ(k-1))$  with  $j, k = 1, \dots, 17$ .

The natural domain for the ordered pair  $\mathbf{p} = (\theta_1, \theta_2)$  is the torus  $T^2 = S^1 \times S^1$ . The joint wind direction distribution is simply the distribution of  $\mathbf{p}$  over  $T^2$ . To ensure the correct toroidal topology we identify the two sets of opposing edges of the grid  $\{\mathbf{x}_{jk}\}$ .

A discrete realisation of the joint wind direction distribution for a pair of stations is then given by the grid-based function

**Table 1**  
Descriptions of the thirteen station locations used in the study.

Location ID	Longitude	Latitude	Elevation	Approx. slope	Approx. aspect	Site description	Sampling period
A1	148.89449	-35.42375	1313 m	0°	NA	Ridge-top site. Sparse acacia seedlings to height of 1 m within a radius of 5–6 m. No canopy overhead.	22/12/2006–17/10/2007
A2	148.89675	-35.42162	1250 m	30–35°	93°	E-facing slope. Sparse acacia seedlings and bracken to 1 m height. Some larger eucalypts approx. 10 m away. Relatively thin canopy.	16/1/2007–17/10/2007
A3	148.89761	-35.42185	1268 m	30–35°	143°	SE-facing slope. Sparse acacia seedlings, bracken and grass up to 1 m high. Some larger eucalypts approx 10 m away with some overhanging branches within 4 m of anemometer. Relatively thin canopy.	16/1/2007–9/3/2007
A4	148.91370	-35.41875	820 m	5–10°	90°	Bottom of main slope, E-facing. Eucalypt regrowth and bracken approx 4–5 m away and some larger eucalypts with cambial growth	9/3/2007–17/10/2007
B1	148.90222	-35.40898	1338 m	0°	NA	approx 6–7 m away. Slightly denser canopy than at A2 and A3. Ridge-top site. Sparse acacia seedlings up to 1 m high and snow-gum regrowth up to 2 m high within a 4 m radius of station. Sparse canopy overhead.	23/1/2007–17/10/2007
B2	148.90442	-35.40876	1277 m	25–30°	148°	SE-facing slope. Sparse bracken and acacia seedlings up to 1.5 m in height. Some small eucalypt regrowth approx. 5 m from station. Light canopy cover.	1/1/2007–17/10/2007
B3	148.90541	-35.40975	1216 m	25–30°	100°	E-facing slope on southern face of scree-gully. Very sparse acacia and grass. Very little to no canopy cover.	19/2/2007–17/10/2007
B4	148.91370	-35.41875	820 m	5–10°	90°	Bottom of main slope, E-facing. Eucalypt regrowth and bracken approx 4–5 m away and some larger eucalypts with cambial growth	9/3/2007–17/10/2007
C1	148.76619	-35.30373	1026 m	0°	NA	approx 6–7 m away. Slightly denser canopy than at B2 and B3. Ridge-top site. Relatively dense acacia seedlings and other regrowth outside of 3 m. Larger eucalypts with cambial growth approx 4–5 m away. Very little canopy immediately overhead but relatively dense canopy over station surrounds.	10/1/2007–16/10/2007
C2	148.77113	-35.29196	955 m	20–25°	105°	E-facing slope on western side of Flea Ck. valley. Sparse eucalypt regrowth approx. 3–4 m from station. Some taller trees, some with cambial growth, approx. 4–5 m from station. Partially intact canopy overhead.	5/1/2007–16/10/2007
C3	148.78222	-35.29232	787 m	5–10°	150°	Near bottom of Flea Ck. valley on small knoll. Some burnt trees approx. 3–4 m away. Scattered canopy overhead.	5/1/2007–16/10/2007
C4	148.78878	-35.28964	850 m	10–15°	300°	W-facing slope near bottom of the eastern sidewall of Flea Ck. valley. Very dense (dead) bracken up to 1 m high. Some larger trees, some with cambial regrowth approx. 5–6 m away. Sparse canopy overhead.	4/1/2007–16/10/2007
C5	148.79787	-35.28990	1000 m	20–25°	315°	NW-facing slope on eastern sidewall of Flea Ck. valley. Very sparse acacia regrowth and bracken within a radius of 5–6 m. Some larger eucalypts 7–8 m from station. Relatively sparse canopy overhead.	4/1/2007–16/10/2007

$$H_{jk} = \sum_{i=1}^M \delta_{jk}^i, \quad j, k = 1, \dots, 17 \quad \text{where}$$

$$\delta_{jk}^i = \begin{cases} 1 & \text{if } \mathbf{p}^i = \mathbf{x}_{jk} \\ 0 & \text{otherwise} \end{cases}$$

We will refer to  $H_{jk}$  as the sampled joint wind direction histogram for the relevant pair of stations.

Given the inherent uncertainties in the data and sources of error associated with field-data collection, the sampled histograms provided by equation should not be considered to be without some form of error. We therefore assume that  $H_{jk}$  is a noisy realisation of a continuous joint wind direction distribution function, that is

$$H_{jk} = g(\mathbf{x}_{jk}) + \varepsilon_{jk}, \quad j, k = 1, \dots, 17,$$

where  $g$  is the continuous (actual) joint wind direction distribution function and  $\varepsilon_{jk}$  is a random error term assumed to be normally distributed with zero mean.

To obtain a more robust estimate of the joint wind direction distribution we use the method of thin-plate smoothing splines (Wahba, 1990). Thin-plate smoothing splines have been used to

extract signals from noisy or erroneous climatological data in many instances; see for example Hutchinson and Bischof (1983), Hutchinson (1995a, 1995b, 1998), Sharples and Hutchinson (2003, 2005), Sharples et al. (2005) and Hennessy et al. (2008). The second-order thin-plate smoothing spline estimate of the joint wind direction distribution function  $g$  is obtained by minimising

$$\frac{1}{n} \sum_{j=1}^{17} \sum_{k=1}^{17} [H_{jk} - f(\mathbf{x}_{jk})]^2 + \lambda J_2(f)$$

over a class of suitably smooth candidate functions  $f$  (Wahba, 1990). Here  $n = 289$ , the number of cells in the grid  $\{\mathbf{x}_{jk}\}$ ,  $\lambda$  is a smoothing parameter and  $J_2(f)$  is the second-order roughness penalty consisting of the integral of squared second-order partial derivatives of  $f$ . In practice, the smoothing spline methods described above are implemented using the “ANUSPLIN” package, a collection of FORTRAN routines for fitting and calculating thin-plate smoothing splines (Hutchinson, 2003).

Due to the measures taken previously, to ensure the toroidal topology of the initial grid, the fitted surfaces possess a structure that is approximately toroidal. We assumed that the final surfaces

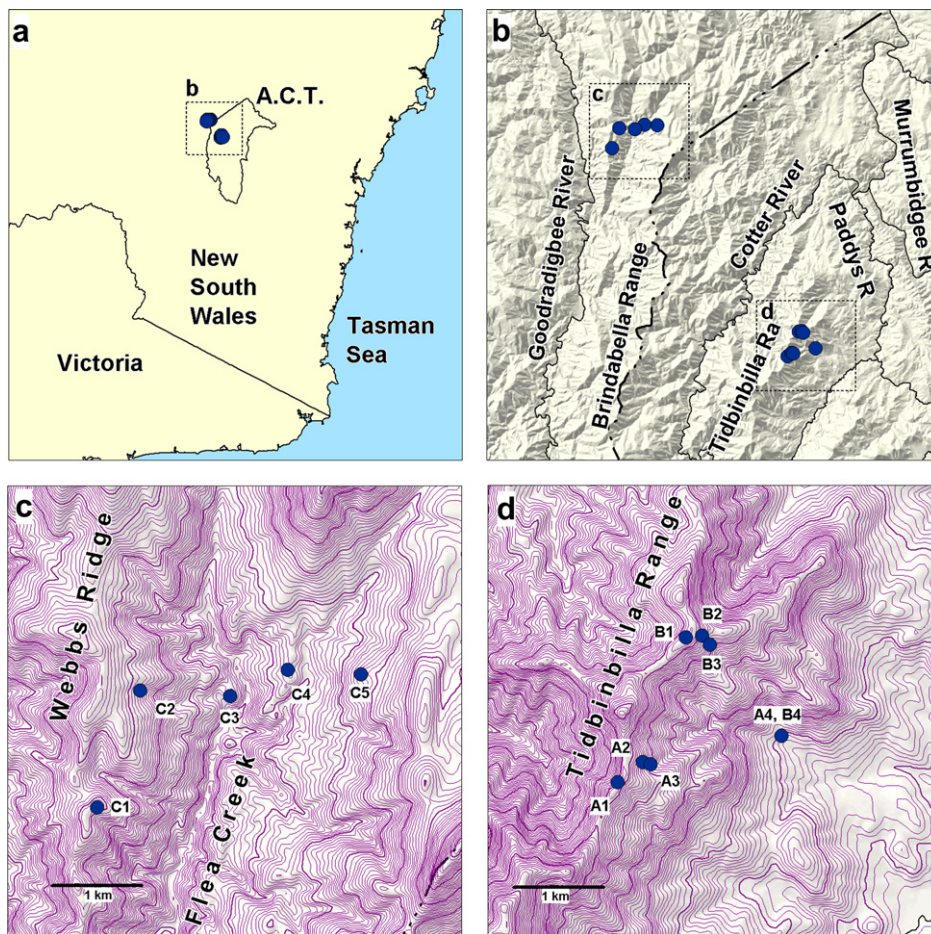


**Fig. 1.** Maps showing the locations of the remotely deployed portable automatic weather stations used in the study. Panel a shows southeastern Australia and the A.C.T. region. Panel b shows the two general study areas. Transect C can be seen in panel c and transects A and B can be seen in panel d. The contours in panels c and d represent the local terrain; major contours are spaced at 100 m, minor contours at 10 m.

were scaled so that the total volume contained under each surface was equal to unity. Each surface can then be interpreted as an estimate of the joint probability distribution for the pair  $\mathbf{p} = (\theta_1, \theta_2)$  over the torus  $T^2$ .

To investigate the effect of wind speed on the various wind-terrain systems the procedure described above was repeated using a number of threshold wind speeds. In these analyses, the wind direction pair was only included in the histogram totals if the first station recorded a simultaneous wind speed greater than or equal to the threshold wind speed. The threshold wind speeds used in the analyses were 0, 2, 4, 6, 8, and 10  $\text{ms}^{-1}$ .

Station pairings were assigned based on the specific transects to which the stations belong. In what follows we will consider ten station pairings, which are listed in Table 2. Also included in Table 2 are the additional six pairings of the Bureau of Meteorology's (BoM) stations CA and MG with the three ridge-top stations. These additional pairings are considered to ascertain how representative the ridge-top wind directions are of the broader-scale wind direction.

## 4. Results

In this section we examine the joint wind direction distributions arising from application of the analytical methods described above. In what follows we will denote the wind speed and direction experienced at X by  $U_x$  and  $\theta_x$ , respectively, where  $X = \text{CA, MG, A1, A2, etc.}$

### 4.1. BoM and ridge top stations

We begin by investigating how 5 m wind direction experienced at the ridge-top locations compares to 10 m wind direction experienced at the BoM automatic weather stations at Canberra Airport (CA) and Mt. Ginini (MG). These two official weather monitoring stations are the closest to the study areas and are separated by a distance of approximately 46 km. These two stations therefore provide a picture of broader scale wind patterns. Comparing data recorded at these two stations with that recorded at the ridge-top stations will provide information on how representative the ridge-top wind directions are of the larg-scale wind patterns.

#### 4.1.1. CA pairings

We first consider the pairings (CA, A1), (CA, B1) and (CA, C1) and derive an estimate of the joint wind direction distribution for each, imposing different threshold wind speeds. The results for the pairings (CA, A1) and (CA, C1) can be seen in Fig. 2. The results for the (CA, B1) pairing were very similar to those for the (CA, A1) pairing, and so will not be discussed.

For the (CA, A1) pairing, all of the joint wind direction distributions are trimodal with modes roughly at (WNW, WNW), (E, E) and (E, W), listing them in order of the most to least dominant. The horizontal bands seen in Fig. 2a indicate that the (one-dimensional) wind direction distribution for the location A1 is manifestly bimodal, even when very slight winds are considered. Note that the banding becomes more fragmented as the wind speed increases; discounting

**Table 2**  
The number of wind direction data pairs for each of the station pairings and for each of the threshold wind speeds analysed.  $U_1$  is used to denote the wind speed measured at the first station in each pairing.

Station pairing	No. of data pairs with $U_1 \geq 0 \text{ ms}^{-1}$	No. of data pairs with $U_1 \geq 2 \text{ ms}^{-1}$	No. of data pairs with $U_1 \geq 4 \text{ ms}^{-1}$	No. of data pairs with $U_1 \geq 6 \text{ ms}^{-1}$	No. of data pairs with $U_1 \geq 8 \text{ ms}^{-1}$	No. of data pairs with $U_1 \geq 10 \text{ ms}^{-1}$
(A1, A2)	9646	6088	2821	827	319	105
(A1, A3)	2473	1570	606	75	7	0
(A1, A4)	7069	4490	2216	754	312	105
(B1, B2)	9332	3957	2429	892	354	57
(B1, B3)	6079	3035	2001	819	338	56
(B1, B4)	6839	3254	2138	859	349	56
(C1, C2)	9552	1580	79	0	0	0
(C1, C3)	9509	1578	78	0	0	0
(C1, C4)	7604	1389	69	0	0	0
(C1, C5)	9689	1578	78	0	0	0
(CA, A1)	5415	5117	2992	1545	53	90
(CA, B1)	4950	4116	2327	1190	397	70
(CA, C1)	5415	4594	2630	1338	453	79
(MG, A1)	5825	5699	3862	1931	700	169
(MG, B1)	4822	4702	3157	1607	598	152
(MG, C1)	5258	5145	3510	1769	647	160

the more erratic light winds reveals the true modes of the paired wind direction system. The two-dimensional mode at (WNW, WNW) in Fig. 2a indicates that when winds at CA satisfy  $250^\circ \leq \theta_{CA} \leq 360^\circ$ , then the winds experienced at A1 will satisfy  $250^\circ \leq \theta_{A1} \leq 315^\circ$  with a high probability. The fact that the horizontal extent of the (WNW, WNW) mode is greater than its vertical extent suggests that the winds at A1 are constrained by the surrounding rugged terrain. This can also be seen, to a lesser extent, in Fig. 2b and c, where only winds at CA that are greater than  $4 \text{ ms}^{-1}$  and  $8 \text{ ms}^{-1}$ , respectively, were considered. The (WNW, WNW) mode seen in Fig. 2a–c implies that, modulo the constraining effect of the topography, the wind directions experienced at A1 and CA are consistent. The same can also be said for the (E, E) mode.

The (E, W) mode, on the other hand, implies that at certain times the wind directions at CA and A1 can be diametrically opposed. To explain this mode we note that it is not uncommon for Canberra to experience a ‘sea breeze’ during summer afternoons (Taylor et al., 2005; Mills, 2007). Fig. 3a shows a plot of the dew point temperature experienced at A1 against the same at CA for all wind direction pairs ( $\theta_{CA}, \theta_{A1}$ ) in the (E, W) mode, i.e. satisfying  $45^\circ \leq \theta_{CA} \leq 135^\circ$  and  $225^\circ \leq \theta_{A1} \leq 315^\circ$ . It is evident that, in the majority, the dew points experienced at CA were significantly higher than those experienced at A1. This is consistent with easterlies pushing into Canberra but not further west into the mountainous study region. Furthermore, Fig. 3b indicates that the wind direction pairs corresponding to the (E, W) mode occur almost exclusively in the afternoon and preferentially in late spring, summer or early autumn which confirms that the (E, W) mode is due to the effects of the ‘sea breeze’ at CA. Hence, by discounting the (E, W) mode, which arises due to the effects of the local sea breeze, we may conclude that the wind directions at CA and A1 are consistent.

Considering the joint distribution functions arising from the (CA, C1) pairing, which can be seen in Fig. 2d–f, we find a similar trimodal structure to that found in considering the (CA, A1) pairing. The (one-dimensional) wind direction distribution for C1 is bimodal with easterly and west-southwesterly modes. The apparent preference for WSW winds at C1 is again most likely due to the influence of the terrain on the wind flow. The near diagonal alignment of the (WNW, WSW) mode suggests that as winds at CA are varied about WNW, the winds at C1 vary about WSW in the same way. That is, a wind at CA that is slightly more northerly (southerly) than WNW will tend to be slightly more northerly (southerly) than WSW at C1. This implies that there is a degree of continuity between wind directions at CA and those at C1. The (E, WSW) mode is analogous to the (E, W) mode in the (CA, A1) pairing and is due to the occurrence

of a sea breeze that penetrates inland to the Canberra region. Thus discounting the local sea breeze effect, the wind directions experienced at CA and C1 are roughly consistent.

#### 4.1.2. MG pairings

We next consider the pairings (MG, A1), (MG, B1) and (MG, C1). The joint wind direction distributions for the (MG, A1) and (MG, C1) pairings can be seen in Fig. 4. The joint distributions for the (MG, B1) pairing were almost identical to those for the (MG, A1) pairing and so will not be shown.

For the (MG, A1) pairing, all of the joint distributions are bimodal, with a dominant mode at (W, WNW) and a secondary mode at (E, E). We note the absence of an (E, W) ‘sea breeze’ mode; MG is further inland and typically beyond the westward extent of the sea breeze infiltration. As can be seen in Fig. 4a–c, both modes lie very close to the dashed line, indicating equal wind direction, and so we can conclude that the wind directions experienced at MG and A1 are consistent. The same can be said for the (MG, C1) pairing, which also exhibits bimodal joint distributions. As can be seen in Fig. 4d–f, both modes again lie very close to the line of equal wind direction and so we can conclude that the wind directions experienced at MG and C1 are roughly consistent.

The above considerations suggest that the wind directions experienced at the ridge-top locations provide a reasonable representation of the broader-scale wind direction. This justifies our use of the ridge-top wind directions as reference wind directions in the analyses of the remaining intra-transect pairings.

#### 4.2. Transect A

The reference wind direction for transect A was provided by the ridge-top station at A1. This station was paired with three other stations at A2, A3 and A4. The details for all these station locations can be found in Table 1 and their positions are shown in Fig. 1.

##### 4.2.1. (A1, A2) pairing

Fig. 5 shows the joint wind direction distributions for the (A1, A2) pairing for each of the threshold wind speed values. All exhibit a definite modal structure. The joint distribution in Fig. 5a, corresponding to all matched pairs (i.e.  $U_{A1} \geq 0 \text{ ms}^{-1}$ ), exhibits four modes located roughly at (WNW, E), (ESE, E), (WNW, WNW) and (SE, NW) with associated modal probabilities of approximately 0.38, 0.34, 0.21 and 0.04, respectively. The (ESE, E) and (WNW, WNW) modes correspond to conditions in which the winds simply flow up and over the ridge line at A1 without any substantial

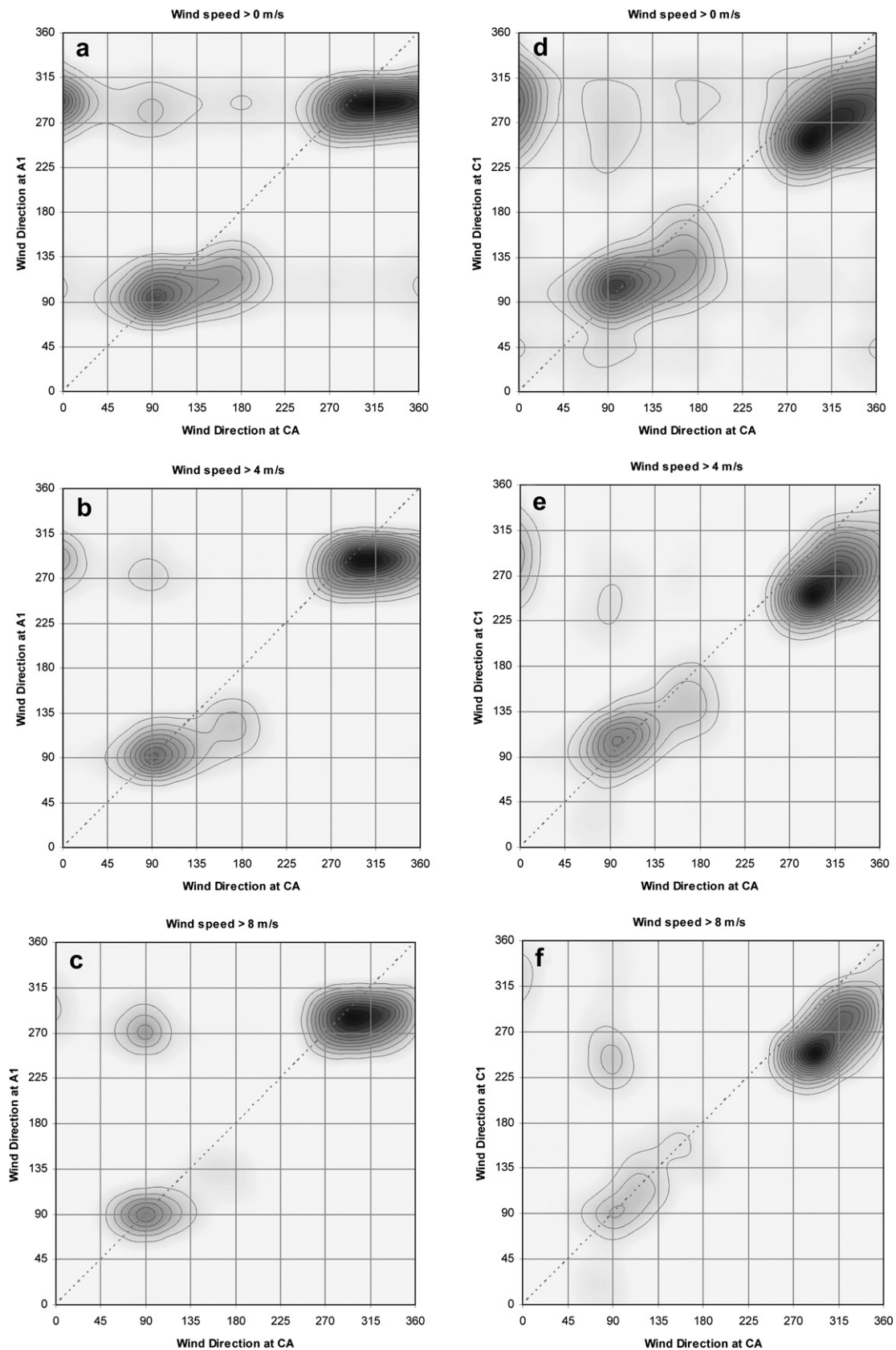


**Fig. 2.** Joint wind direction distributions for CA and A1 (panels a–c) and for CA and C1 (panels d–f). The first row corresponds to all matched pairs; the second and third rows correspond to matched pairs for which the wind speed at CA was greater than  $4 \text{ ms}^{-1}$  and  $8 \text{ ms}^{-1}$ , respectively. Darker colouring indicates higher frequency. The contours are included only to give a better indication of the shape of the surface. The dashed line indicates equal wind direction at the two stations.

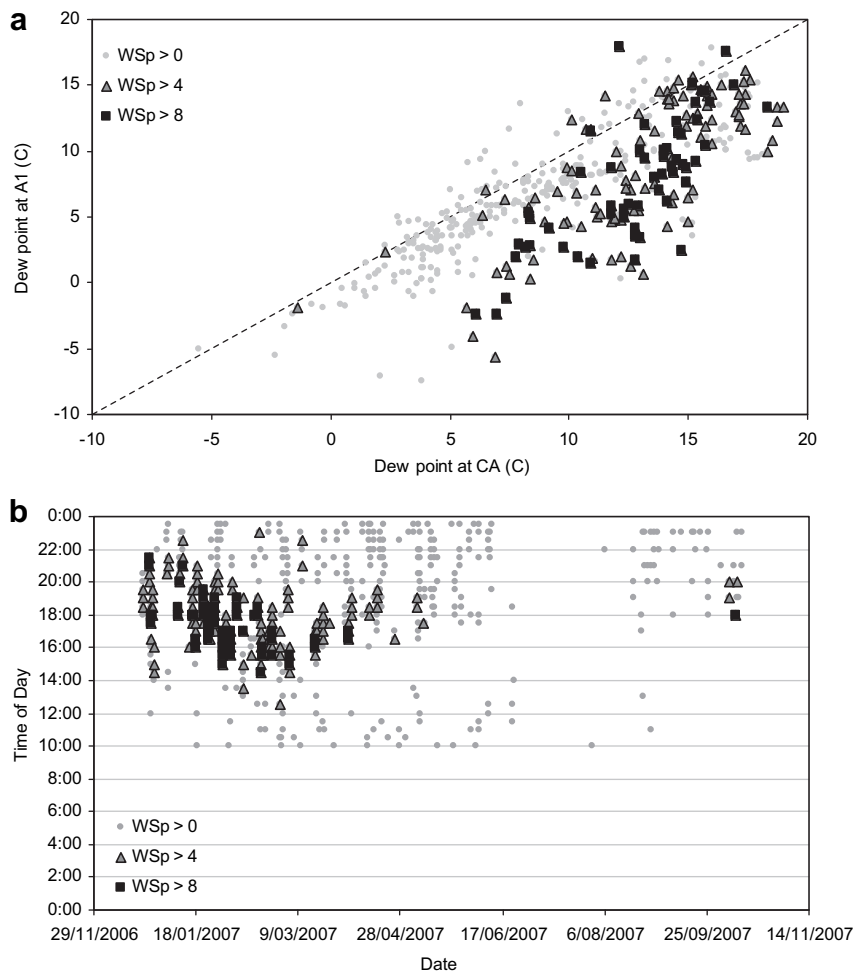


**Fig. 3.** (a) Plot of dew point at A1 against simultaneous dew point at CA for all wind direction pairs ( $\theta_{CA}$ ,  $\theta_{A1}$ ) in the (E, W) mode, i.e. satisfying  $45^\circ < \theta_{CA} < 135^\circ$  and  $225^\circ < \theta_{A1} < 315^\circ$ . The different symbols correspond to different threshold wind speeds. (b) Scatter-plot of the times and dates corresponding to the points in panel (a).

change in the wind direction. The vertically distended shape of the modes indicates that there is greater variance in the wind direction at A2, due to the various local gullies and spur lines. Increased turbulence is another possible explanation for the distended shape.

Increasing the threshold wind speed changes the modal structure of the corresponding joint distributions, as can be seen in Fig. 5. Fig. 6 illustrates how the modal probabilities respond as the threshold wind speed is varied. In particular, the mode at (SE, NW) has completely vanished when  $U_{A1} \geq 4 \text{ ms}^{-1}$ . The dates and times corresponding to the (SE, NW) mode, defined by  $80^\circ \leq \theta_{A1} \leq 160^\circ$  and  $260^\circ \leq \theta_{A2} \leq 360^\circ$ , indicated that such conditions occur preferentially during the night-time. In fact only about 4% of events corresponding to the (SE, NW) mode occurred between 08:00 and 16:00 h. Hence the (SE, NW) mode, and its disappearance as the threshold wind speed is increased, is consistent with the occurrence of a weak nocturnal drainage flow, which is overcome by stronger ambient winds.

As the threshold wind speed is increased the (WNW, E) mode dominates. The likelihood associated with the (WNW, WNW) mode drops substantially for  $U_{A1} \geq 4 \text{ ms}^{-1}$  with a complementary rise in the likelihood of the (WNW, E) mode. In fact as the wind speed threshold rises above  $8 \text{ ms}^{-1}$  the joint wind direction distribution becomes unimodal at (WNW, E). Note that due to the toroidal structure the (WNW, E) mode ‘wraps around’ from the bottom to the top of the figures. The fact that this mode dominates for high wind speeds across the ridge at A1 is interesting as it indicates that the winds at A1 and A2 are often opposed, despite the fact that they

are within a few hundred metres of each other. Considering Fig. 5 and f further, it is apparent that when a WNW wind of  $8 \text{ ms}^{-1}$  or more is flowing across the ridge at A1, the wind direction at A2 can be anywhere between  $0^\circ$  and  $180^\circ$  with a high likelihood of it falling between NNE and ESE. These conditional probabilities will be quantified further in the next section.

It is well known that diurnal heating and cooling of rugged landscapes can induce thermal winds that flow downslope just after sunset and upslope at sunrise (Whiteman, 2000). It is therefore possible that the (WNW, E) mode could be due to thermally-driven upslope winds. In our study region winds that arise due to this effect would be expected to be slight and occur during daylight hours. Fig. 7 a and b, however, suggest that the data corresponding to the (WNW, E) mode cannot all be due to these diurnal winds. Fig. 7a and b indicate that the winds at A1 and A2 can be opposed for extended periods of up to 5 or 6 days, as indicated by the unbroken vertical bands in the figures. Moreover, the unbroken vertical bands in Fig. 7a and b mostly occur for higher wind speeds. The wind data represented by these vertical bands are unlikely to be due to thermally-driven winds (which would typically occur for only several hours during the day). It is more likely that these data correspond to the occurrence of a lee-slope eddy, which is a mechanically generated effect. As a consequence, the winds experienced at the surface on the lee-slope would be opposed to the ridge-top wind direction. The distended shape of the (WNW, E) mode in Fig. 2 suggest that these thermal and eddy-driven winds

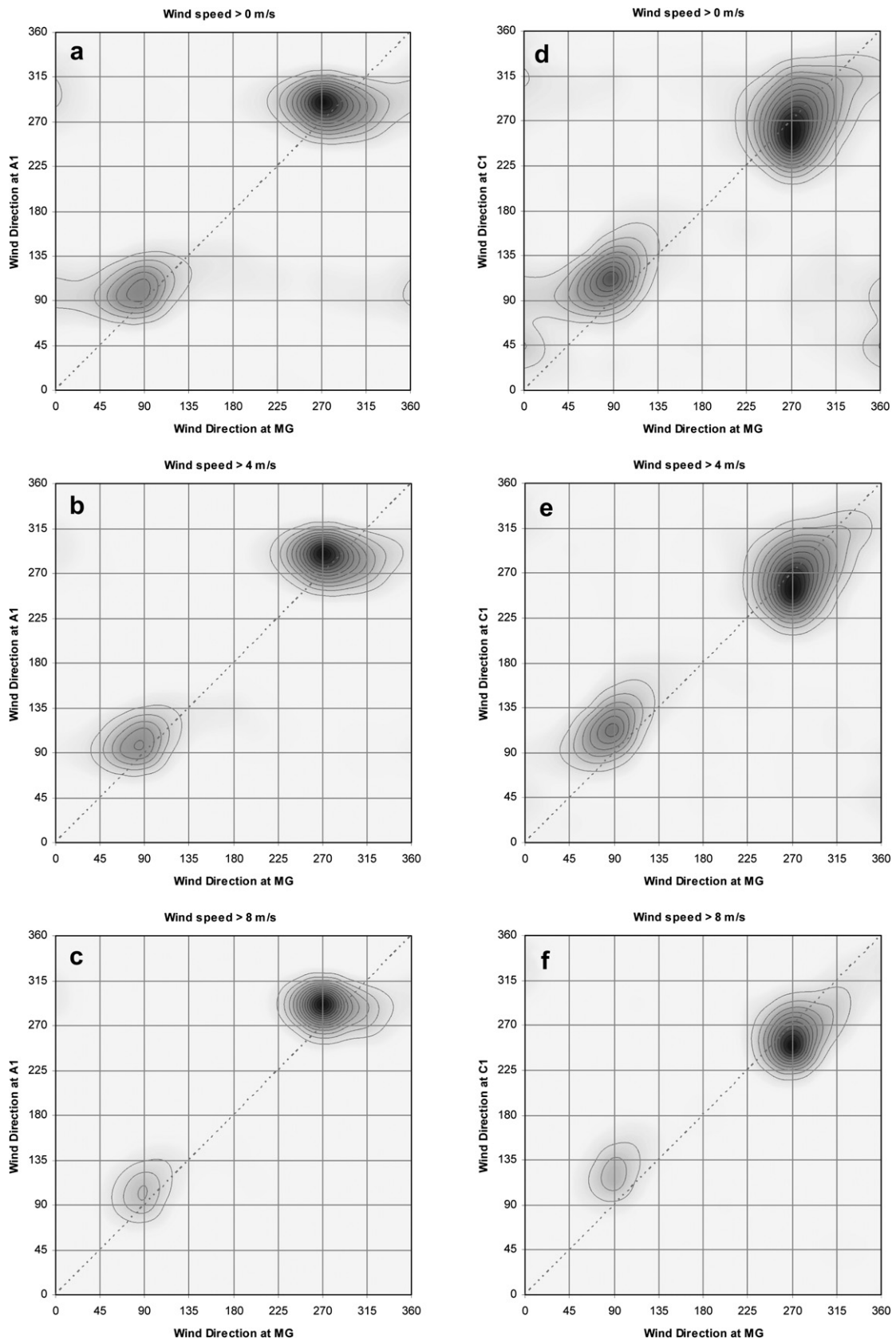


**Fig. 4.** Joint wind direction distributions for MG and A1 (panels a–c) and for MG and C1 (panels d–f). The first row corresponds to all matched pairs; the second and third rows correspond to matched pairs for which the wind speed at MG was greater than  $4 \text{ ms}^{-1}$  and  $8 \text{ ms}^{-1}$ , respectively. Darker colouring indicates higher frequency. The contours are included only to give a better indication of the shape of the surface. The dashed line indicates equal wind direction at the two stations.

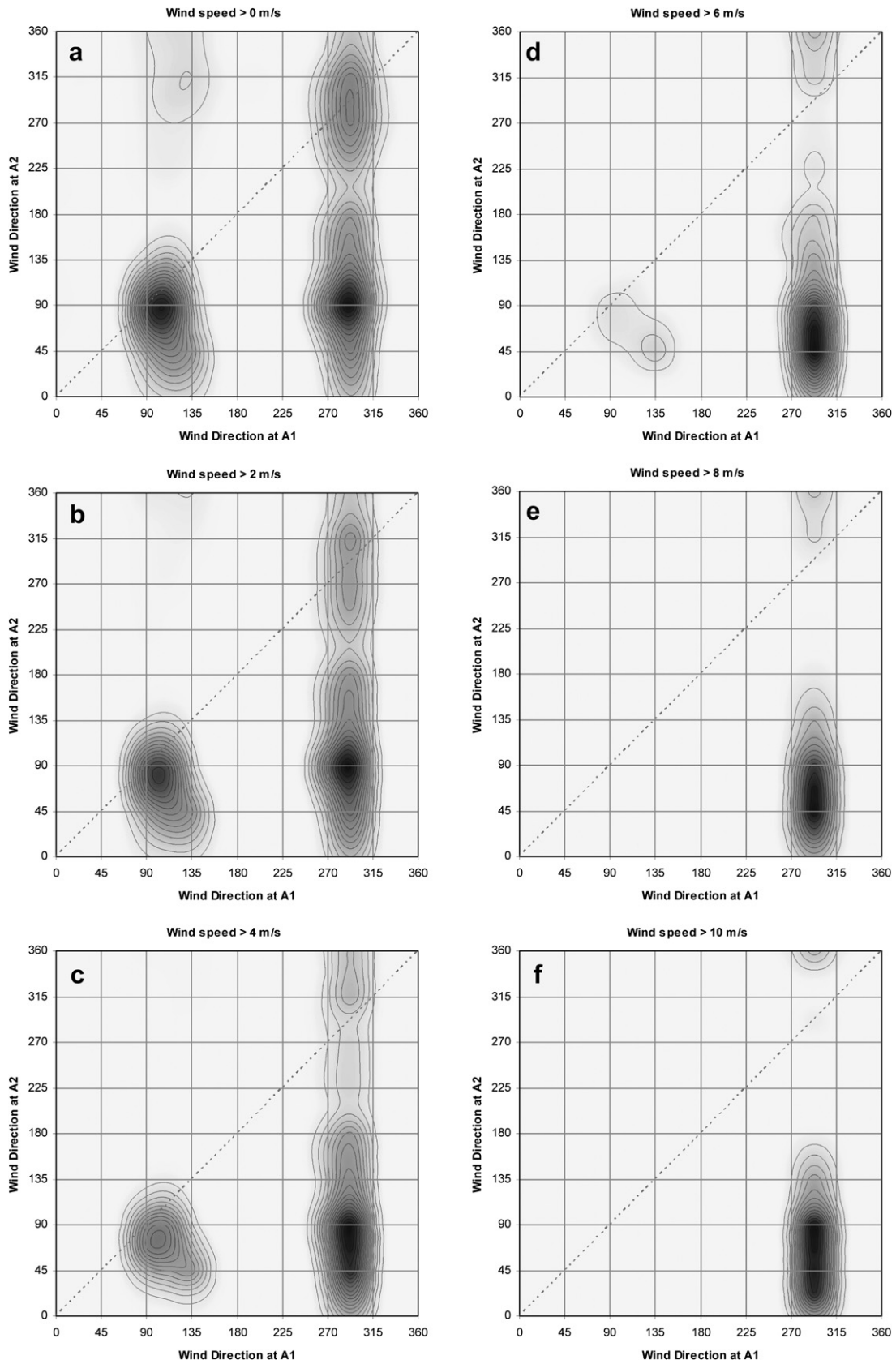


**Fig. 5.** Joint wind direction distributions for A1 and A2 assuming different threshold wind speeds: (a)  $0 \text{ ms}^{-1}$  (all matched pairs), (b)  $2 \text{ ms}^{-1}$ , (c)  $4 \text{ ms}^{-1}$ , (d)  $6 \text{ ms}^{-1}$ , (e)  $8 \text{ ms}^{-1}$  and (f)  $10 \text{ ms}^{-1}$ . Darker colouring indicates higher frequency. The contours are included only to give a better indication of the shape of the surface. The dashed line indicates equal wind direction at A1 and A2.

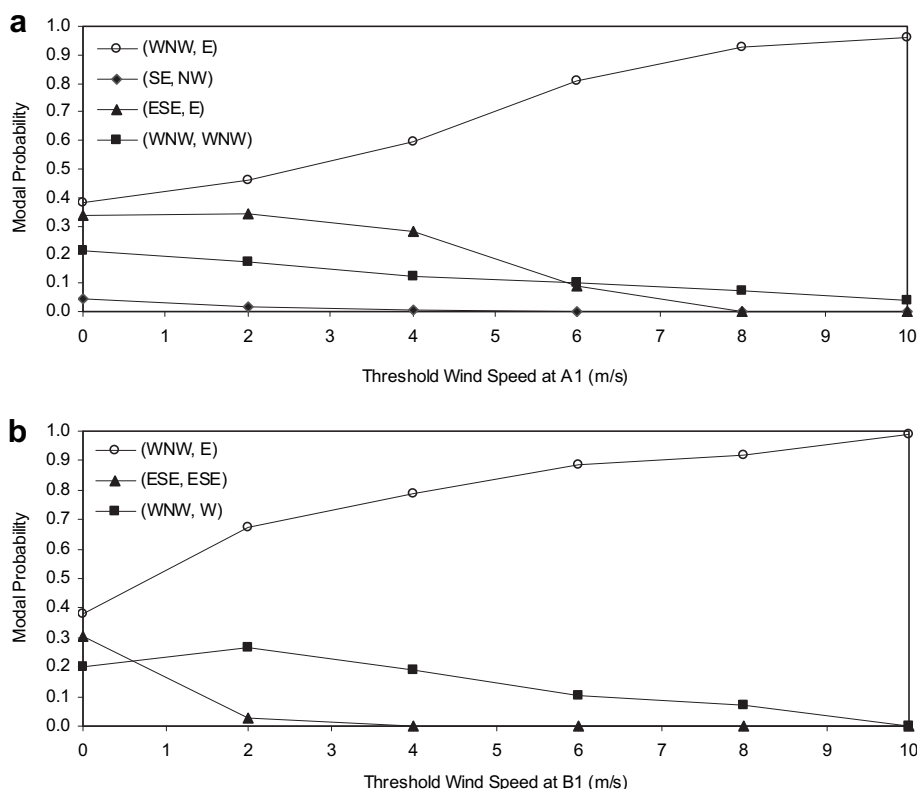


**Fig. 6.** Plots showing how modal probabilities for the (A1, A2) and (B1, B2) pairings respond to varying threshold wind speed. (a) For the (A1, A2) pairing the modes are defined by: (WNW, E) =  $\{(\theta_{A1}, \theta_{A2}) \in T^2: 245^\circ \leq \theta_{A1} \leq 335^\circ \text{ and } 0^\circ \leq \theta_{A2} \leq 210^\circ\}$ ; (ESE, E) =  $\{(\theta_{A1}, \theta_{A2}) \in T^2: 60^\circ \leq \theta_{A1} \leq 160^\circ \text{ and } 0^\circ \leq \theta_{A2} \leq 160^\circ\}$ ; (WNW, WNW) =  $\{(\theta_{A1}, \theta_{A2}) \in T^2: 245^\circ \leq \theta_{A1} \leq 335^\circ \text{ and } 210^\circ \leq \theta_{A2} \leq 360^\circ\}$ ; (SE, NW) =  $\{(\theta_{A1}, \theta_{A2}) \in T^2: 80^\circ \leq \theta_{A1} \leq 160^\circ \text{ and } 260^\circ \leq \theta_{A2} \leq 360^\circ\}$ . (b) For the (B1, B2) pairing the modes are defined by: (WNW, E) =  $\{(\theta_{B1}, \theta_{B2}) \in T^2: 252^\circ \leq \theta_{B1} \leq 332^\circ \text{ and } 5^\circ \leq \theta_{B2} \leq 165^\circ\}$ ; (ESE, ESE) =  $\{(\theta_{B1}, \theta_{B2}) \in T^2: 60^\circ \leq \theta_{B1} \leq 190^\circ \text{ and } 57^\circ \leq \theta_{B2} \leq 187^\circ\}$ ; (WNW, W) =  $\{(\theta_{B1}, \theta_{B2}) \in T^2: 240^\circ \leq \theta_{B1} \leq 350^\circ \text{ and } 210^\circ \leq \theta_{B2} \leq 360^\circ\}$ .

can also have an across slope component at times, presumably resulting in an overall helical motion above the slope.

The distributions for the (A1, A3) pairing were quite similar in structure to those for the (A1, A2) pairing, and indicated a high likelihood of wind reversal at A3 when it is on the lee side of the ridge. This is not surprising since the locations A2 and A3 are only approximately 60 m apart.

#### 4.2.2. (A1, A4) pairing

In Fig. 8 the joint wind direction distributions for the (A1, A4) pairing indicate a more complex wind-terrain interaction, with six identifiable modes. In Fig. 8a the joint distribution possesses a mode located at (ESE, W) indicating that wind at A4 can flow downslope against the bulk winds. This situation could occur during night-time due to the drainage of cool air into lower areas such as that in which A4 is located. Fig. 9a shows the dates and times corresponding to the data pairs in the (ESE, W) mode, i.e.  $75^\circ \leq \theta_{A1} \leq 165^\circ$  and  $232^\circ \leq \theta_{A4} \leq 352^\circ$ . As can be seen, the majority of data pairs in the (ESE, W) mode occur between 16:00 h and 09:00 h, which is consistent with them being due to a nocturnal drainage flow. By contrast, the dates and times corresponding to data pairs in the (WNW, NE) mode follow quite a different pattern. Fig. 9b indicates that conditions contributing to this mode often occur during daylight hours, but can persist for several days. The pattern in Fig. 9b is similar to that seen in Fig. 7a and b for the (A1, A2) pairing.

A comparison of the dates and times corresponding to the (WNW, E) mode for the (A1, A2) pairing and the (WNW, NE) mode for (A1, A4) pairing indicated a high degree of coincidence. This is a strong indication that these analogous modes arise due to the same processes, most likely upslope thermal winds and lee-eddies.

The additional modes for the (A1, A4) pairing, located at (ESE, S) and (WNW, S), indicate the likelihood of differences in wind direction of approximately  $90^\circ$  at A1 and A4. Examination of the dates and times corresponding to the (WNW, S) mode indicated that such conditions occurred preferentially during daylight hours (approx. 10:00–18:00 h) with only sporadic and fleeting events taking place in the night. The timing of these events suggests the existence of a thermal upslope wind from the south at A4. This is plausible since there is a spur with a steep southerly-facing sidewall just to the north of A4, which could provide the thermal differences required to produce such a flow. The dates and times corresponding to the (ESE, S) mode exhibited a slight preference for daytime occurrence, again consistent with a thermal upslope wind, but also indicated that conditions in this mode can persist for a day or two. This suggests that these persistent conditions are not linked with any diurnal process. Further examination of the dates and times showed that it was mostly these persistent events that were contributing to the (ESE, S) mode for higher threshold wind speeds. Dynamic channelling of broad-scale east-south-easterlies could be responsible for these types of persistent events.

#### 4.3. Transect B

The reference wind direction for transect B was provided by the ridge-top station at B1. This station was paired with three other stations at B2, B3 and B4. The details for all these station locations can be found in Table 1 and their positions are shown in Fig. 1.

##### 4.3.1. (B1, B2) pairing

Joint wind direction distributions for the (B1, B2) pairing can be seen in Fig. 10a–c. All exhibit a definite modal structure. In

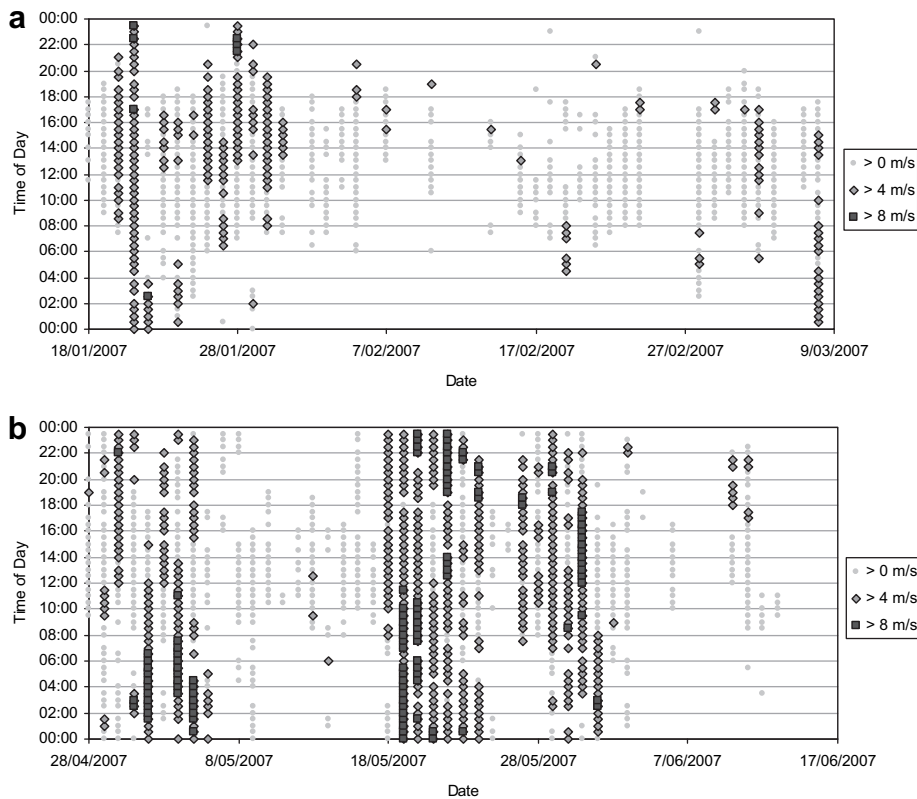


**Fig. 7.** Diagnostic plots for the (WNW, E) mode of the joint wind direction distribution for the (A1, A2) pairing. The (WNW, E) mode is defined by  $245^\circ \leq \theta_{A1} \leq 335^\circ$  and  $0^\circ \leq \theta_{A2} \leq 210^\circ$ . (a) Plot showing dates (18th Jan–9th Mar 2007) and times corresponding to the (WNW, E) mode. (b) Plot showing dates (28th Apr–17th Jun 2007) and times corresponding to the (WNW, E) mode.

particular, the (B1, B2) pairing exhibits modes at (WNW, E), (WNW, W) and (ESE, ESE). As the threshold wind speed is increased the (ESE, ESE) and (WNW, W) modes deteriorate; the (ESE, ESE) mode vanishes when  $U_{B1} \geq 4 \text{ ms}^{-1}$  (Fig. 10b) and the (WNW, W) mode vanishes when  $U_{B1} \geq 10 \text{ ms}^{-1}$  (Fig. 10c). As  $U_{B1}$  increases the (WNW, E) mode becomes more focused towards (WNW, ENE). The dates and times corresponding to the (WNW, E) mode, defined by  $252^\circ \leq \theta_{B1} \leq 332^\circ$  and  $5^\circ \leq \theta_{B2} \leq 165^\circ$ , were checked against those corresponding to the (WNW, E) mode for the (A1, A2) pairing by means of a plot similar to those in Fig. 7a and b. A strong coincidence was found between the two sets of dates and times, indicating that these corresponding modes in the (A1, A2) and (B1, B2) pairings are due to the same processes, thermally-driven upslope winds and lee-slope eddy occurrence.

The modal response curves, showing how the modal probabilities for the (B1, B2) pairing vary as the threshold wind speed is increased, can be seen in Fig. 6b. It is evident that the (WNW, E) dominates for higher ambient wind speeds, with a complementary fall in the probability associated with the (WNW, W) mode for ambient wind speeds above  $4 \text{ ms}^{-1}$ . This is a very similar response to that of the (WNW, E) and (WNW, WNW) modes for the (A1, A2) pairing (Fig. 6a). Fig. 6b, however, indicates that winds satisfying  $\theta_{A1}, \theta_{B1} \approx \text{WNW}$  are slightly more likely to flow down the slope at B2 than at A2.

#### 4.3.2. (B1, B3) pairing

The joint wind direct distributions for the (B1, B3) pair can be seen in Fig. 10d–f. The joint distribution for all matched pairs exhibits definite modes centred near (WNW, SSE), (WNW, WNW) and (ESE, S). Inspection of the dates and times corresponding to the (ESE, S) mode, defined by  $75^\circ \leq \theta_{B1} \leq 175^\circ$  and  $125^\circ \leq \theta_{B3} \leq 235^\circ$ , revealed that conditions contributing to this mode would often

persist for several days. This suggests that this mode is due to mechanical forcing rather than diurnal thermal effects (Whiteman, 2000). It is likely that the ESE ambient winds are channelled by the windward terrain resulting in southerly winds at B3.

The conditions corresponding to the (WNW, SSE) mode, defined by  $245^\circ \leq \theta_{B1} \leq 335^\circ$  and  $75^\circ \leq \theta_{B3} \leq 215^\circ$ , were also seen to persist over several days and exhibited a strong coincidence with the dates and times corresponding to the (WNW, E) mode of the (A1, A2) pairing. Hence, the SSE winds at B3, which occur when winds at B1 are roughly WNW, are most likely due to the effects of a lee eddy. The more southerly wind direction observed at B3 (e.g. as compared to that at B2), is possibly due to a finer-scale terrain channelling of the recurved winds blowing back up the slope. It could be argued that the (WNW, SSE) and (WNW, WNW) modes in the joint distribution for all matched pairs ( $U_{B1} \geq 0 \text{ ms}^{-1}$ ) are in fact part of the same mode that extends over  $250^\circ \leq \theta_{B3} \leq 360^\circ$ . As the wind speed threshold is increased the (WNW, WNW) component of this extended mode retracts towards the north, while the (WNW, SSE) component is stable with respect to wind speed. This suggests that as wind speed increases it is less likely for winds satisfying  $\theta_{B1} \approx \text{WNW}$  to flow over the ridge without separating from the surface in the lee near B3.

Not surprisingly, the joint wind directions for the (B1, B4) pairing (not shown) exhibited a very similar structure to those for the (A1, A4) pairing, with six identifiable modes. Only three of these modes persisted when  $U_{B1} \geq 2 \text{ ms}^{-1}$ , all satisfying  $250^\circ \leq \theta_{B1} \leq 330^\circ$ .

#### 4.4. Transect C

The reference wind direction for transect C was provided by the ridge-top station at C1. This station was paired with four other

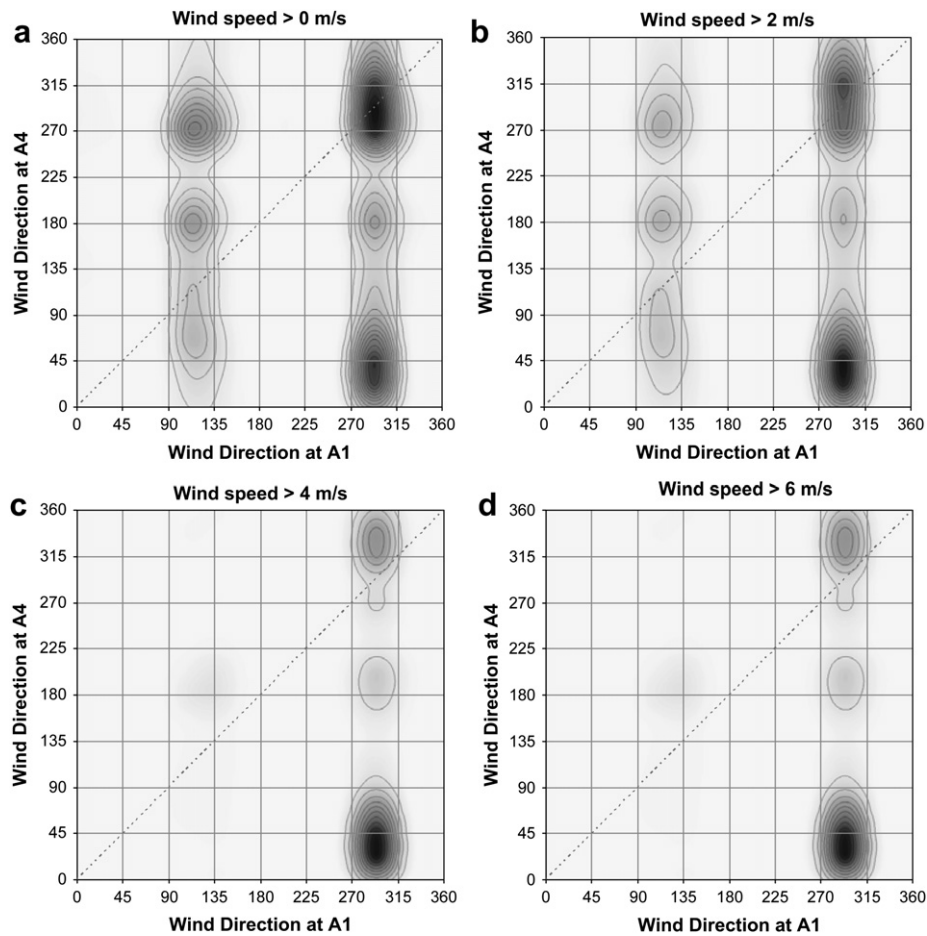


Fig. 8. Joint wind direction distributions for the (A1, A4) pairing. (a) All matched wind direction pairs,  $U_{A1} \geq 0 \text{ ms}^{-1}$ , (b)  $U_{A1} \geq 2 \text{ ms}^{-1}$ , (c)  $U_{A1} \geq 4 \text{ ms}^{-1}$ , (d)  $U_{A1} \geq 6 \text{ ms}^{-1}$ .

stations at C2, C3, C4 and C5. The details for all these station locations can be found in Table 1 and their positions are shown in Fig. 1. Owing to the thicker vegetation in its vicinity, the maximum wind speed recorded at C1 was only  $5.8 \text{ ms}^{-1}$ .

#### 4.4.1. (C1, C2) pairing

The joint wind direction distributions for the (C1, C2) pairing can be seen in Fig. 11a–c. The  $U_{C1} \geq 0 \text{ ms}^{-1}$  joint distribution exhibits two prominent modes roughly located at (ESE, E) and (W, ESE), and several more diffuse modes, most notably near (WNW, WNW). As the threshold wind speed is increased beyond  $2 \text{ ms}^{-1}$  only the two modes near (ESE, E) and (W, ESE) remain, with the (W, ESE) mode registering the highest relative frequency. This indicates that when ambient winds are strong and westerly, the winds at C2 will be reversed with near certainty. Note that as the threshold wind speed is increased the mode at (W, ESE) tends more toward (WSW, ESE) due to changes in the wind characteristics at C1 for higher wind speeds. The modal probabilities are summarised in Table 3.

The (ESE, E) mode corresponds to an approximately easterly ambient wind that flows up and over the slope at C2 and the ridge at C1, while the (W, ESE) mode corresponds to the occurrence of lee-eddies or thermally-driven upslope winds at C2 when the ambient winds are from an approximately westerly direction. The fact that the (WNW, WNW) mode vanishes indicates that when the ambient winds are stronger, there is very little net flow passing over the ridge and moving down the slope at C2. Presumably these winds are separating from the surface in the lee of the ridge.

Diagnostic plots (not shown) indicated that conditions corresponding to the (W, ESE) mode of the  $U_{C1} \geq 2 \text{ ms}^{-1}$  joint distribution

for the (C1, C2) pairing were mostly coincident with conditions corresponding to the (WNW, E) mode of the  $U_{A1} \geq 2 \text{ ms}^{-1}$  joint distribution for the (A1, A2) pairing. This demonstrates that the ambient conditions were producing a consistent effect on similar terrain elements even though they were separated by more than 10 km.

#### 4.4.2. (C1, C3) pairing

The joint wind direction distributions for the (C1, C3) pairing, shown in Fig. 11d–f, exhibit a different modal structure than those for the (C1, C2) pairing. For the  $U_{C1} \geq 0 \text{ ms}^{-1}$  distribution there are four modes located approximately at (ESE, NNE), (WNW, N), (W, SW) and (SSE, SSW). Note that the (ESE, NNE) and (WNW, N) modes wrap around from the bottom to the top in Fig. 11d and e. As the threshold wind speed at C1 is increased there are three stable modes. For ambient wind speeds satisfying  $U_{C1} \geq 4 \text{ ms}^{-1}$  the modes centred at (WSW, NE) and (SE, NE) dominate with associated probabilities of about 46% and 35%, respectively. The probability associated with the (ESE, S) mode increases slightly from around 6% to 10% as the ambient wind speed measured at C1 is increased from 0 to  $4 \text{ ms}^{-1}$ .

The dates and times corresponding to the (WSW, NE) mode for the (C1, C3) pairing were found to share a high degree of coincidence with those corresponding to the (W, ESE) mode for the (C1, C2) pairing – only 8 out of 472 dates and times for the (C1, C3) pairing were not included in the dates and times for the (C1, C2) pairing.

Conditions corresponding to the (W, SW) mode for the (C1, C3) pairing occurred preferentially during the day during summer and early to mid-autumn. During the winter months, conditions corresponding to the (W, SW) mode occurred during both day and night,

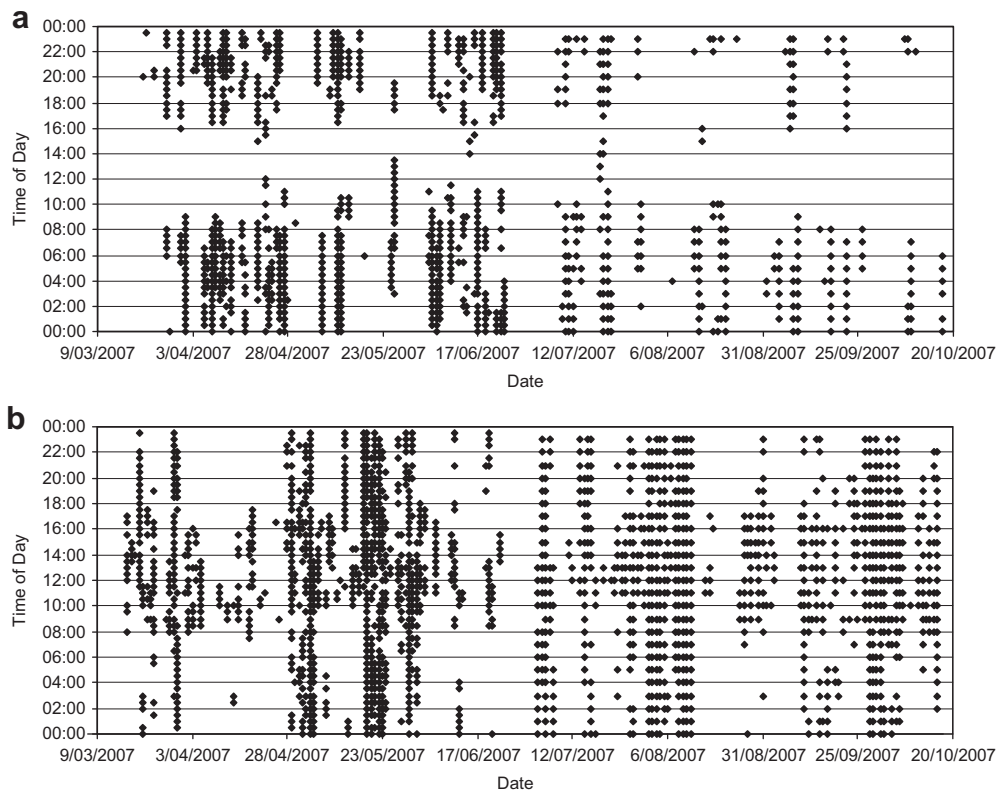


**Fig. 9.** Diagnostic plots for the (WNW, NE) and (ESE, W) modes of the joint wind direction distribution for the (A1, A4) pairing. All matched pairs (i.e.  $U_{A1} \geq 0 \text{ ms}^{-1}$ ) have been included in the plots: (a) Plot of time of day against date (9th Mar 2007–20th Oct 2007) for data contributing to the (ESE, W) mode, (b) Plot of time of day against date (9th Mar 2007–20th Oct 2007) for data contributing to the (WNW, NE) mode. The (WNW, NE) mode is defined by  $252^\circ \leq \theta_{A1} \leq 332^\circ$  and  $0^\circ \leq \theta_{A4} \leq 120^\circ$  and the (ESE, W) mode is defined by  $75^\circ \leq \theta_{A1} \leq 165^\circ$  and  $232^\circ \leq \theta_{A4} \leq 352^\circ$ .

and in some cases persistently over one or two days. Winter events associated with threshold wind speeds satisfying  $U_{C1} \geq 2 \text{ ms}^{-1}$  did appear to occur more during daylight hours, however. The dates and times corresponding to data in the (SSE, SSW) mode displayed a less distinctive pattern. During summer and early autumn conditions corresponding to this mode occur fleetingly during both day and night-time hours. From mid-autumn to late winter only three or four events occurred with conditions corresponding to the (SSE, SSW) mode. In all cases the event persisted over a number of days.

The location C3 sits at the lowest point in the cross-valley transect, just near the junction of two tributaries. The down-valley direction is aligned roughly between south and southwest (see Fig. 1c). The results cited above therefore fit with the existence of valley winds driven by thermal differences or mechanical forcing. Examination of the dates and times corresponding to the various modes suggested the existence of thermally-driven up-valley winds during warmer months and forced channelling of bulk westerlies along Flea Creek during winter.

To further test for the existence of along-valley winds, particular focus was directed at conditions corresponding to  $\theta_{C3} \approx \text{N}$ . We considered two sets of data. The first set contained pairs satisfying  $0^\circ \leq \theta_{C1} \leq 212^\circ$  and  $280^\circ \leq \theta_{C3} \leq 20^\circ$ , while the second contained pairs satisfying  $214^\circ \leq \theta_{C1} \leq 354^\circ$  and  $315^\circ \leq \theta_{C3} \leq 20^\circ$ . Diagnostic plots (not shown) of the dates and times associated with these pairs indicated that when  $0^\circ \leq \theta_{C1} \leq 212^\circ$  (roughly north to south-southwest), the northerly winds experienced at C3 occurred predominantly during the night-time. This is consistent with a nocturnal down-valley wind. A similar but less distinct pattern was found for the case  $214^\circ \leq \theta_{C1} \leq 354^\circ$  (roughly south-southwest to north). A majority of the events occurred in the night-time but

some events did occur sporadically during daylight hours and are thus unlikely to be thermally-driven down-valley winds. Dynamic channelling of bulk westerlies down the valley to the north of C3 could be candidate mechanisms for these northerly winds at C3.

#### 4.4.3. (C1, C4) pairing

The joint wind direction distributions for the (C1, C4) pairing can be seen in Fig. 12a–c. The  $U_{C1} \geq 0 \text{ ms}^{-1}$  joint distribution for the (C1, C4) pairing exhibits a prominent mode roughly located at (W, WNW), and several more diffuse modes near (WNW, ENE), (S, ENE), (W, SW) and (E, NW). As the threshold wind speed is increased beyond  $2 \text{ ms}^{-1}$  the modes near (WNW, ENE) and (S, ENE) vanish, the mode near (E, NW) deteriorates and an additional mode becomes distinguishable at (E, S). Examination of the dates and times corresponding to the (W, WNW) mode indicated the presence of an upslope wind at C4 driven by a combination of thermal effects and the momentum of bulk winds from the west. For wind speeds satisfying  $U_{C1} \geq 2 \text{ ms}^{-1}$  the probability associated with the (W, WNW) mode is roughly 50%.

The dates and times corresponding to the (WNW, ENE) mode displayed a distinctly different pattern to that for the (W, WNW) mode. Conditions corresponding to the (WNW, ENE) mode displayed a strong preference for occurrence during night-time hours, with only about 5% of events occurring between 10:00 and 16:00 h. The (WNW, ENE) mode is thus likely due to the occurrence of a relatively weak nocturnal drainage flow that can move in opposition to the ambient winds when they are slight but whose effect is overcome by stronger ambient winds. This assertion is further supported by the fact that the valley above C4 is aligned in an approximately north-easterly direction (see Fig. 1c). The mode at (S,

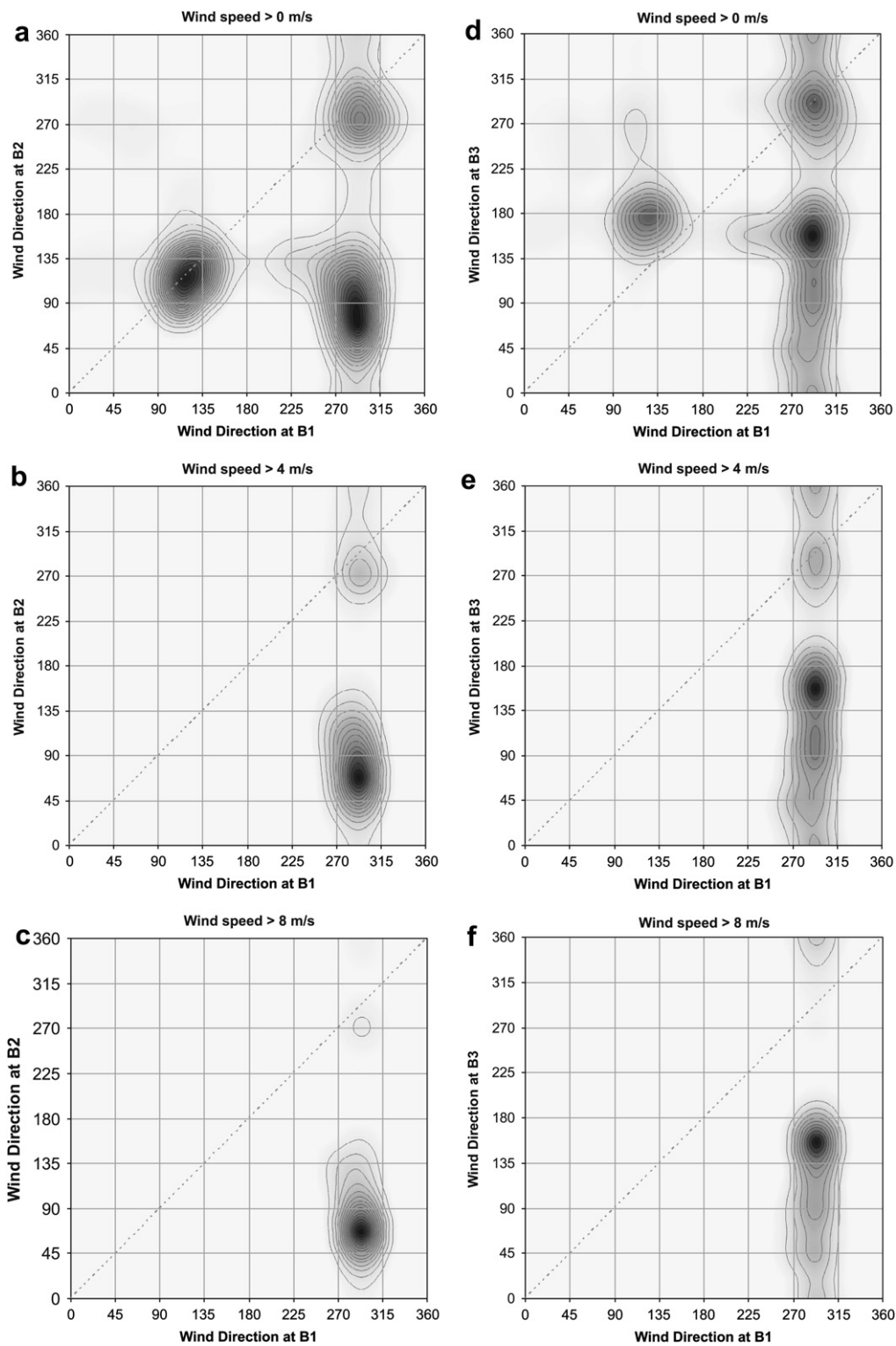


**Fig. 10.** Joint wind direction distributions for B1 and B2 (panels a–c) and for B1 and B3 (panels d–f). Panels (a) and (d) correspond to all matched pairs, panels (b) and (e) correspond to matched pairs satisfying  $U_{B1} \geq 4 \text{ ms}^{-1}$  and panels (c) and (f) correspond to matched pairs satisfying  $U_{B1} \geq 8 \text{ ms}^{-1}$ .

ENE) is also due to occurrence of nocturnal drainage flow at C4, with most of the corresponding times falling between 16:00 and 10:00 h.

The times and dates pertaining to the (W, SW) mode for the (C1, C4) pairing shared a similar pattern with those of the (W, SW) mode for the (C1, C3) pairing, which has been discussed previously. Hence,

the (W, SW) mode for the (C1, C4) pairing is most likely due to the occurrence of up-valley winds and some forced channelling of winds up the Flea Creek valley. The pattern of dates and times for the (E, NW) mode suggests a process, or set of processes, that persists over extended periods of up to 4–5 days. Dates and times corresponding to this mode were compared with those corresponding to

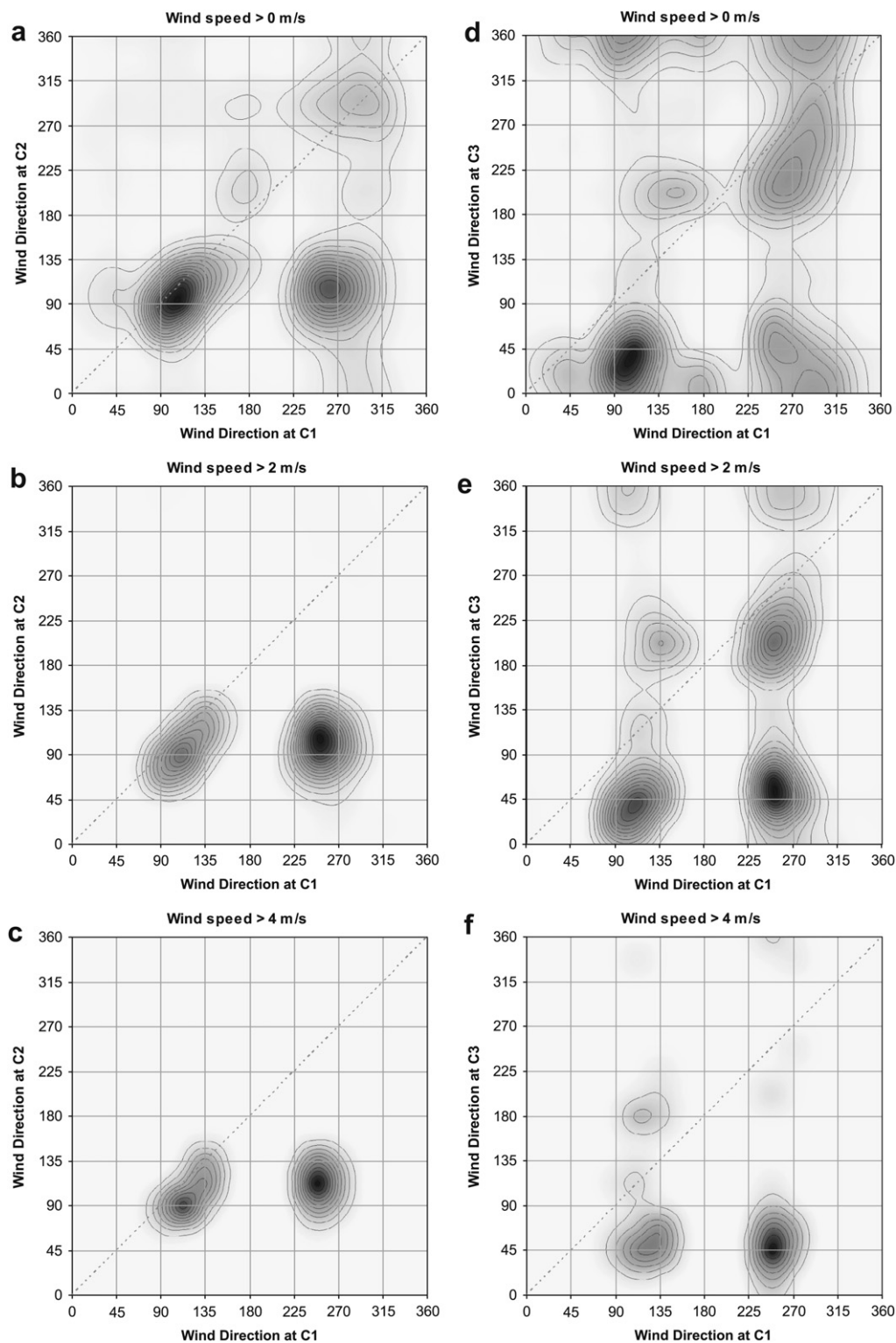


**Fig. 11.** Joint wind direction distributions for C1 and C2 (panels a–c) and for C1 and C3 (panels d–f). Panels (a) and (d) correspond to all matched pairs, panels (b) and (e) correspond to matched pairs satisfying  $U_{C1} \geq 2 \text{ ms}^{-1}$  and panels (c) and (f) correspond to matched pairs satisfying  $U_{C1} \geq 4 \text{ ms}^{-1}$ .

the (SSE, SSW) mode of the (C1, C3) pairing and a high degree of coincidence was found. Forced channelling of easterlies down the Flea Creek valley is thus a likely explanation for both of these modes. However, it is important to note that the head of the Flea Creek valley splits into two tributaries; one roughly in a north-south direction and one directed northeast–southwest. These terrain features could

also possibly influence the modal structure apparent in some of the joint distributions, particularly those for the (C1, C3) and (C1, C4) pairings. For example, some of the instances contributing to the (E, NW) mode for the (C1, C4) pairing could be due to thermally-driven drainage winds flowing down the north-south directed tributary above C4.

**Table 3**

Modal probabilities for the (C1, C2) distributions. The modes are defined as follows: (W, ESE) =  $\{(\theta_{C1}, \theta_{C2}) \in T^2: 207^\circ \leq \theta_{C1} \leq 333^\circ \text{ and } 25^\circ \leq \theta_{C2} \leq 175^\circ\}$ ; (ESE, E) =  $\{(\theta_{C1}, \theta_{C2}) \in T^2: 15^\circ \leq \theta_{C1} \leq 195^\circ \text{ and } 25^\circ \leq \theta_{C2} \leq 165^\circ\}$ ; (WNW, WNW) =  $\{(\theta_{C1}, \theta_{C2}) \in T^2: 205^\circ \leq \theta_{C1} \leq 345^\circ \text{ and } 227^\circ \leq \theta_{C2} \leq 357^\circ\}$ .

Wind speed	Modal probability		
	(W, ESE)	(ESE, E)	(WNW, WNW)
$U_{C1} \geq 0 \text{ ms}^{-1}$	0.31594	0.35570	0.15562
$U_{C1} \geq 2 \text{ ms}^{-1}$	0.56939	0.40636	0.01121
$U_{C1} \geq 4 \text{ ms}^{-1}$	0.50580	0.49380	0.00000

#### 4.4.4. (C1, C5) pairing

Fig. 12d–f show that the joint wind direction distributions for the (C1, C5) pairing have three prominent modes near (W, W), (E, NE) and (E, NW). The modal probabilities for this pairing are summarised in Table 4.

The dates and times corresponding to the (W, W) and (E, NE) modes indicated that these modes were due to upslope and downslope winds combining with the ambient flow. The pattern of dates and times corresponding to the (E, NW) mode was less conclusive but indicated that conditions contributing to this mode occurred in a series of persistent events interspersed with events that lasted several hours at a time. During summer these short-lived events showed a slight preference for night-time occurrence, while during winter these shorter events showed a preference for daylight hours. The daytime events are consistent with a thermally-driven upslope flow while the night-time ones could be due to decoupling of the winds at the two stations due to a nocturnal inversion. The persistent events are likely due to the occurrence of a lee-slope eddy at C5 when bulk winds are from the east. In this respect it is interesting to note the symmetry in the joint distributions for the (C1, C2) pairing and the (C1, C5) pairing, which describe the joint wind systems on opposite sides of the valley.

## 5. Implications for bushfire risk management

Bushfire or wildfire risk management agencies often utilise fire spread simulation models as a key part of their decision making processes. These models allow fire managers to gauge how a fire will spread under certain meteorological conditions, enabling them to better prioritise deployment of resources during fire suppression activities. Fire spread models are also used to conduct hypothetical studies that inform broader risk management strategies. Typically these models are sensitive to meteorological variables, particularly wind speed and direction.

Many models combine information on ambient wind speed and direction and terrain characteristics to estimate a terrain-modified wind field. The main problem of interest is typically considered as follows: Given an ambient wind speed and direction, determine the corresponding wind speed and direction at some point in the landscape. The study detailed above directly addresses the directional aspect of this problem. Indeed, the first coordinate in the wind direction pairs treated above was chosen to be indicative of the ambient wind direction, while the second described the directional response of the wind-terrain system at a particular point in the landscape. The study described above therefore provides information of direct relevance to fire managers and fire spread modellers and also provides information that can be used in validating and developing new and existing methods for deriving terrain-modified winds, with wider applications.

As an example of how the results might be employed in bushfire risk management practices, consider the (A1, A2) pairing and suppose that the ambient winds are from the west-northwest. This prompts us to focus on the (univariate) conditional probability distribution defined by taking the  $\theta_{A1} = \text{WNW}$  (vertical) cross-

section of the (A1, A2) joint distribution. Fig. 13a shows the conditional probability distributions associated with threshold wind speeds of 0, 4 and 10  $\text{ms}^{-1}$ . It is apparent that the most likely wind direction at A2 is not WNW. The most likely wind direction is in fact closer to E, but as the ambient wind speed increases, winds satisfying  $\text{NNE} \leq \theta_{A2} \leq \text{E}$  occur with almost equal probability. This finding implies that fire spread models, which assume a constant wind direction throughout the entire region of interest, could be seriously in error when employed in regions possessing complex terrain. The conditional distributions provide guidance on what the most probable wind direction at A2 would be.

Fig. 13b shows the  $\theta_{B1} = \text{WNW}$  conditional probability distributions at B2. A similar trend to that seen in Fig. 13a is evident with ENE winds the most likely at B2. The similar structure evident in Fig. 13a and b suggests that one could extrapolate the result, with reasonable accuracy, to similar terrain elements in the landscape. The slopes listed in Table 1 indicate that significant evidence for lee-eddy occurrence was found when the slope was over 20–25°, which is consistent with the threshold value of 20° reported by Wood (1995). This implies the following general advice: when the wind is from the WNW, it is highly probable that slopes over about 20°, which are approximately east-facing, will experience upslope winds. This probability increases as the ambient wind speed increases.

The conditional probability distributions in Fig. 13a and b also indicate that deterministic methods based on single inputs such as ambient wind speed and direction will not be able to capture the totality of the joint wind direction system. The terrain can cause a WNW wind to respond in different ways depending on the precise conditions of the day or night. For example, Fig. 13a implies that when the wind at A1 satisfies  $U_{A1} \geq 10 \text{ ms}^{-1}$  and  $\theta_{A1} = \text{WNW}$ , the wind at A2 can satisfy  $30^\circ \leq \theta_{A2} \leq 50^\circ$  or  $70^\circ \leq \theta_{A2} \leq 90^\circ$  with almost equal probability; 0.18 or 0.17, respectively. Thus deterministic methods used for deriving terrain-modified winds, which don't incorporate additional relevant information such as time of day or the likelihood of lee-eddies, would not be able to emulate this type of system behaviour. For example, mass consistent methods, which are unable to produce nonlinear effects such as flow reversals on lee-slopes, could produce greatly misleading results (unless the initialising data includes measurements inside a lee-eddy). Calculations based on the conditional distributions indicate that mass consistent methods could be in error over 75% of the time for moderate ambient winds, and over 80% of the time when winds are stronger. If all the significantly relevant processes are not accounted for, accuracy of predictions will degrade. However, for wind in complex terrain, the relevant processes will vary from case to case and information relating to them may not always be readily available. Thus in many instances in fire management and research, models are used to predict terrain-altered winds using only wind speed and direction as inputs. The analysis presented above suggests that such an approach can result in predictions that can be dangerously inaccurate.

In many cases the ambient winds can also experience small directional changes due to local terrain forcing or perturbations in the geostrophic forces driving the winds. This means that it is not always possible to define a single ambient wind direction with certainty. In these cases it is perhaps best to specify a mean wind direction and an associated variance. Alternatively, one could use the joint wind direction distributions, or portions of them if appropriate, with a Monte Carlo approach, reselecting from the distribution at each time step, for example. Another approach is to simply assume that the ambient wind direction occupies some range. For example, suppose that the ambient wind direction satisfies  $W \leq \theta_{A1}, \theta_{B1} \leq \text{NW}$ . The joint wind direction distributions can then be used to calculate the conditional probabilities associated with a range of wind direction responses.

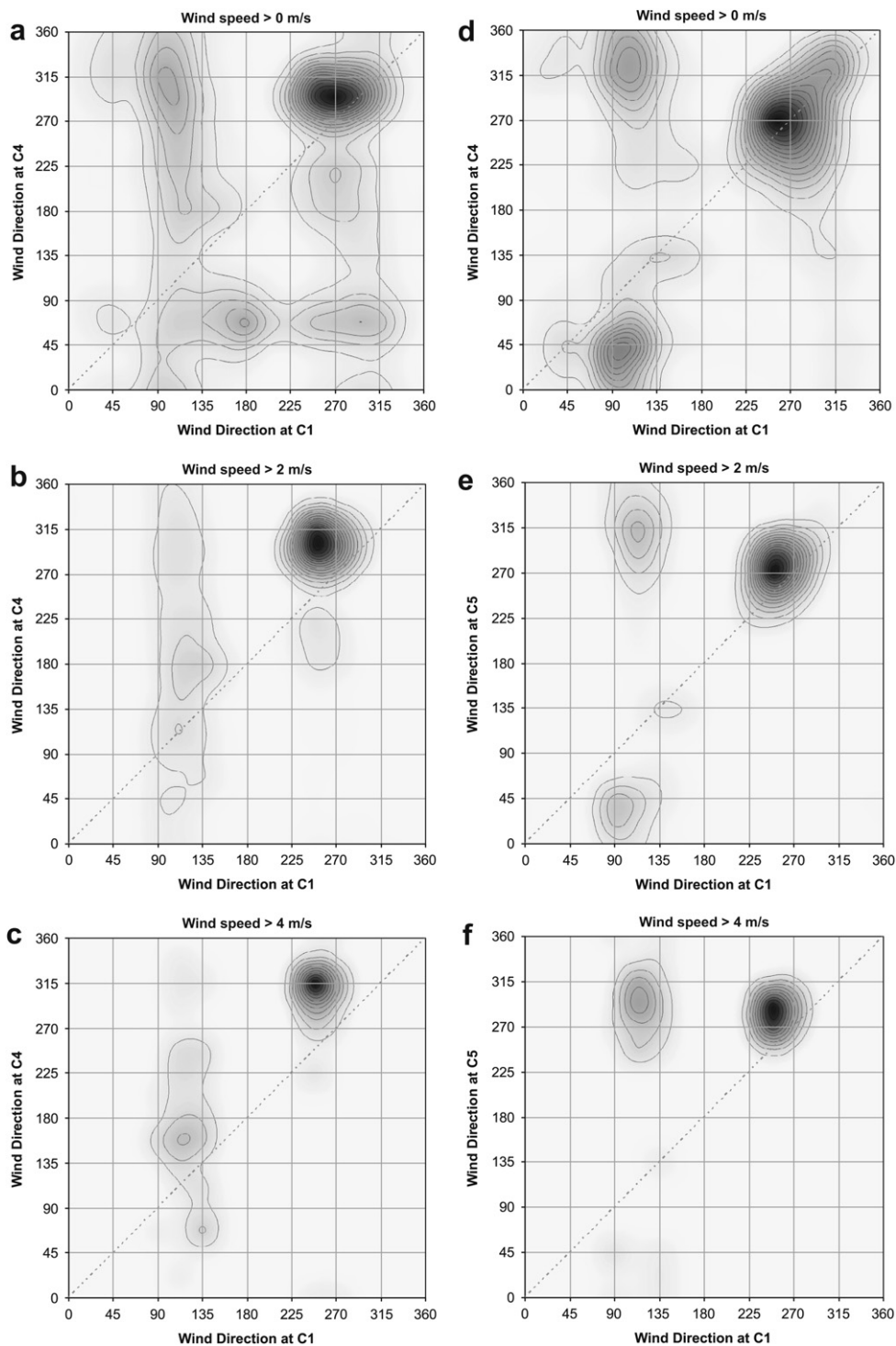


Fig. 12. Joint wind direction distributions for C1 and C4 (panels a–c) and for C1 and C5 (panels d–f). Panels (a) and (d) correspond to all matched pairs, panels (b) and (e) correspond to matched pairs satisfying  $U_{C1} \geq 2 \text{ ms}^{-1}$  and panels (c) and (f) correspond to matched pairs satisfying  $U_{C1} \geq 4 \text{ ms}^{-1}$ .

Fig. 14a shows how the probability of a wind reversal on the east-facing slopes varies with the threshold wind speed measured at A1 and B1. Specifically, Fig. 14a shows the conditional probabilities  $P(\text{NE} \leq \theta_{A2} \leq \text{SE} | \text{W} \leq \theta_{A1} \leq \text{NW})$  and  $P(\text{NE} \leq \theta_{B2} \leq \text{SE} | \text{W} \leq \theta_{B1} \leq \text{NW})$  for different threshold wind speeds, where we have used the notation  $P(A|B)$  to denote the conditional probability of A given B. Similarly, Fig. 14b shows the probability of a wind reversal on either side of the Flea Creek valley for threshold

winds speeds of 0, 2 and  $4 \text{ ms}^{-1}$ . The conditional probabilities represented here are  $P(\text{ENE} \leq \theta_{C2} \leq \text{SSE} | \text{SW} \leq \theta_{C1} \leq \text{W})$  and  $P(\text{WSW} \leq \theta_{C5} \leq \text{NNW} | \text{E} \leq \theta_{C1} \leq \text{SE})$ . In all of these cases there is an overall increase in the conditional probabilities as the threshold wind speed is increased.

As another example, consider the (C1, C3) pairing, which pertains to a location near the bottom of the Flea Creek transect. If we suppose that the ambient winds satisfy  $\text{SW} \leq \theta_{C1} \leq \text{W}$ , then we

**Table 4**

Modal probabilities for the (C1, C5) distributions. The modes are defined as follows: (W, W) =  $\{(\theta_{C1}, \theta_{C5}) \in T^2: 200^\circ \leq \theta_{C1} \leq 350^\circ \text{ and } 160^\circ \leq \theta_{C5} \leq 360^\circ\}$ ; (E, NE) =  $\{(\theta_{C1}, \theta_{C5}) \in T^2: 15^\circ \leq \theta_{C1} \leq 165^\circ \text{ and } 0^\circ \leq \theta_{C5} \leq 100^\circ\}$ ; (E, NW) =  $\{(\theta_{C1}, \theta_{C5}) \in T^2: 35^\circ \leq \theta_{C1} \leq 185^\circ \text{ and } 200^\circ \leq \theta_{C5} \leq 360^\circ\}$ .

Wind speed	Modal probability		
	(W, W)	(E, NE)	(E, NW)
$U_{C1} \geq 0 \text{ ms}^{-1}$	0.50350	0.18776	0.19360
$U_{C1} \geq 2 \text{ ms}^{-1}$	0.60320	0.14407	0.20919
$U_{C1} \geq 4 \text{ ms}^{-1}$	0.54299	0.07134	0.37052

can calculate the conditional probabilities  $P(\text{NNE} \leq \theta_{C3} \leq \text{ESE} | \text{SW} \leq \theta_{C1} \leq \text{W})$  and  $P(\text{SSE} \leq \theta_{C3} \leq \text{WSW} | \text{SW} \leq \theta_{C1} \leq \text{W})$ , the first of which relates the probability of a wind direction that opposes the ambient winds ( $\theta_{C3} \approx \text{ENE}$ ), while the second relates to the probability of winds blowing up Flea Creek valley due to channelling or diurnal effects ( $\theta_{C3} \approx \text{SSW}$ ). Fig. 14c shows these conditional probabilities for threshold wind speeds of 0–4  $\text{ms}^{-1}$ . Fig. 14c indicates that for lower ambient wind speeds the wind direction at C3 can satisfy  $\theta_{C3} \approx \text{ENE}$  or  $\theta_{C3} \approx \text{SSW}$  with almost equal probability. However, for higher ambient wind speeds the wind direction is much more likely to satisfy  $\theta_{C3} \approx \text{ENE}$ . With this sort of information fire managers can better decide how to deploy fire crews and other resources. For example in this case it would seem unwise to put fire-crews immediately to the north or west of C3, even in light winds; a spot fire near C3 could spread up the

eastern face of Webbs Ridge or up the Flea Creek valley, with near equal probability of approximately 30–40%.

The increased likelihood of winds opposing the ambient wind direction at C3, as wind speed increases, is presumably due to the preferential occurrence of a large lee-slope eddy. Indeed this was a likely mechanism for all of the wind reversals observed on lee-slopes (e.g. at A2, A3, B2, B3, C2, etc.), particularly for high ambient wind speeds and events that persisted for extended periods. The results of the analyses also indicate that a lee-eddy can encompass the entire slope. In particular, the presence of modes corresponding to lee-slope eddies in the (A1, A4) and (B1, B4) distributions indicate that under westerly ambient winds a lee-eddy could extend for over a kilometre to the east of the Tidbinbilla range. Similarly, the presence of lee-slope eddies at C3, as indicated in the (C1, C3) distributions, suggests that a lee-eddy can extend all the way to the bottom of a valley, in this case approximately 800–900 m.

In the context of fire management and suppression, lee-slope eddies are a dangerous phenomenon. A theoretical analysis undertaken by Byron-Scott (1990) implied that the rotor motion associated with lee-slope eddies could be accelerated by the presence of a fire. In some cases the effect could produce lee-wind speeds that exceed the ambient wind speed. The turbulence associated with these rotor winds can also lead to increased generation of embers, which due to the accelerated lee-winds can be deposited much further downwind than would otherwise be expected. Unpublished results, arising from numerical simulations conducted by one of the authors (JJS), support the conclusions of Byron-Scott (1990).

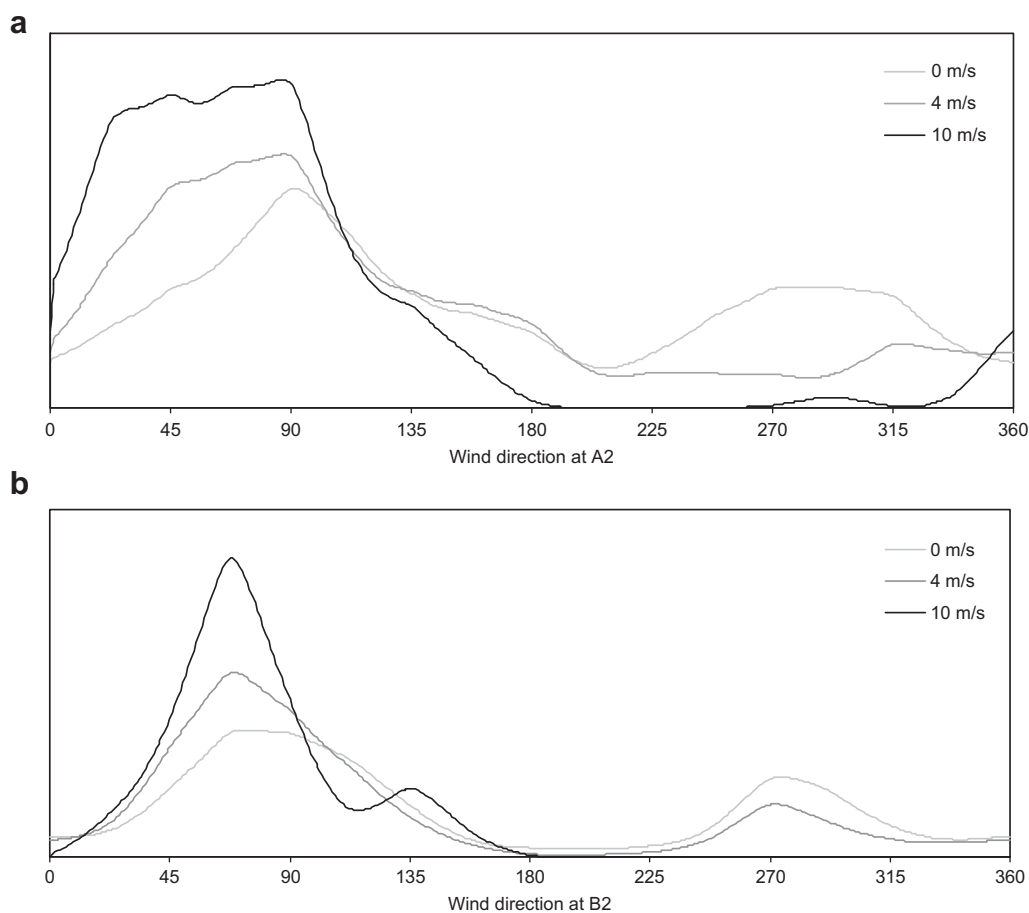


**Fig. 13.** Conditional probability distributions for threshold wind speeds of 0, 4 and 10  $\text{ms}^{-1}$ . (a) Wind direction distributions ( $\theta_{A2}$ ) conditioned on  $\theta_{A1} = \text{WNW}$ , (b) Wind direction distribution ( $\theta_{B2}$ ) conditioned on  $\theta_{B1} = \text{WNW}$ .

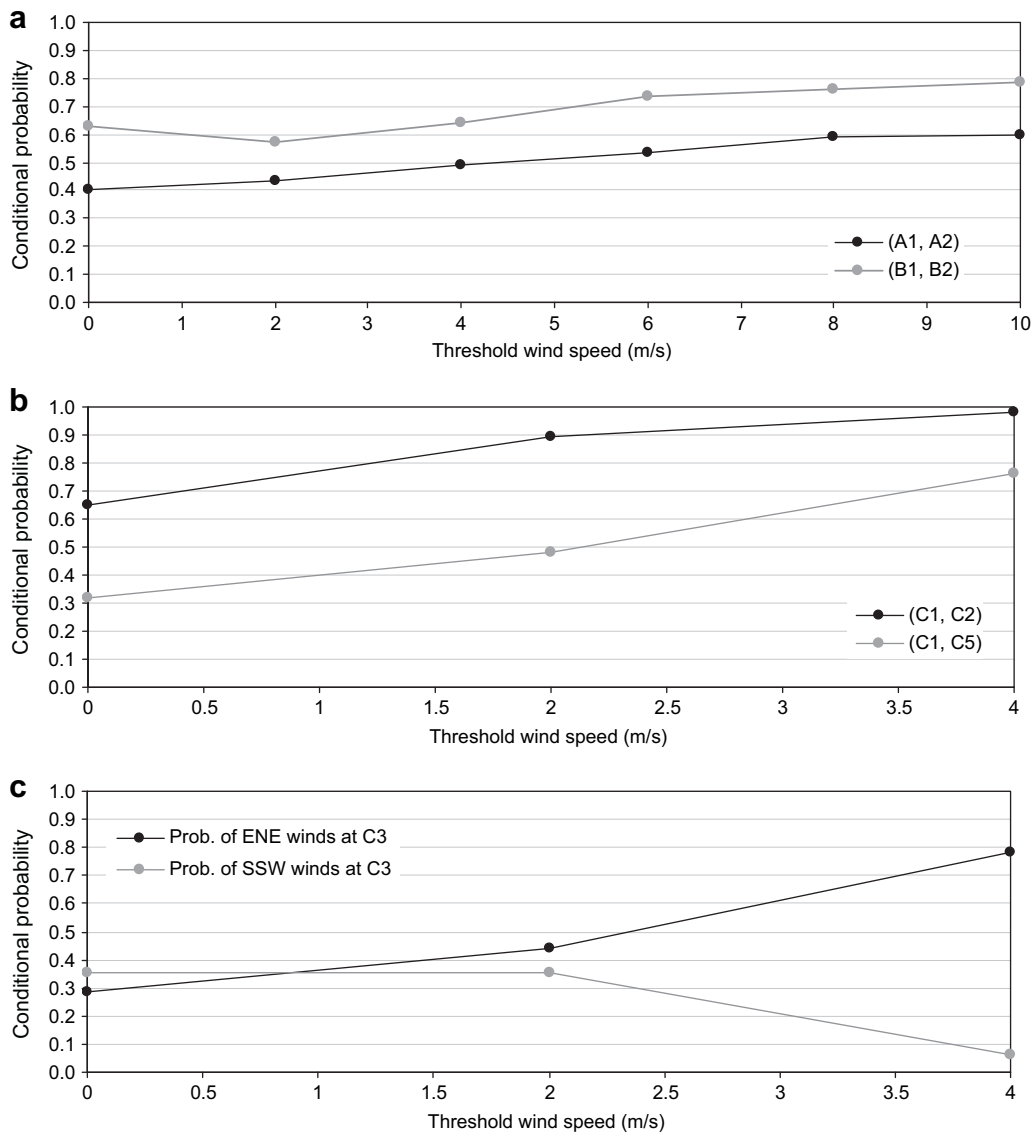


**Fig. 14.** (a) Conditional probabilities  $P(\text{NE} \leq \theta_{A2} \leq \text{SE} | W \leq \theta_{A1} \leq \text{NW})$  (black) and  $P(\text{NE} \leq \theta_{B2} \leq \text{SE} | W \leq \theta_{B1} \leq \text{NW})$  (grey) for different threshold wind speeds 0–10  $\text{ms}^{-1}$ . (b) Conditional probabilities  $P(\text{ENE} \leq \theta_{C2} \leq \text{SSE} | \text{SW} \leq \theta_{C1} \leq \text{W})$  (black) and  $P(\text{WSW} \leq \theta_{C5} \leq \text{NNW} | \text{E} \leq \theta_{C1} \leq \text{SE})$  (grey) for different threshold wind speeds 0–4  $\text{ms}^{-1}$ . (c) Conditional probabilities  $P(\text{NNE} \leq \theta_{C3} \leq \text{ESE} | \text{SW} \leq \theta_{C1} \leq \text{W})$  (black) and  $P(\text{SSE} \leq \theta_{C3} \leq \text{WSW} | \text{SW} \leq \theta_{C1} \leq \text{W})$  (grey) for threshold wind speeds 0–4  $\text{ms}^{-1}$ .

Lee-slope eddies have also been mentioned in connection with rapid lateral spread of fires in rugged terrain. Multispectral imagery of the fire complex to the west of Canberra on the 18th of January 2003 shows regions of intense fire activity characterised by spot fires forming laterally and downwind of fires burning on lee-slopes. Analyses of overlapping images taken at different times indicate that such a process is a very efficient mechanism for carrying fire in rugged terrain. The interaction of a lee-eddy or along-valley channelling, very low fuel moisture and an active fire is a likely explanation for the observed behaviour (McRae, 2004; McRae et al., 2006). The prevalence of lee-eddies and channelling processes, as indicated in the analyses presented above, suggests that a large majority of rugged landscapes may be susceptible to such a process. This claim is further supported by results arising from studies concerning the extreme bushfires that impacted Victoria during February 2009. Indeed, Bradstock and Price (2010) report that the most severe fire behaviour, as indicated by the state of the burnt vegetation, was connected with lee aspects.

The existence of mechanically-forced up-valley winds at C3 ( $\theta_{C3} \approx \text{SSW}$ ) can also be dangerous in the context of fire suppression and crew safety. Suppose a fire, driven by westerly winds, is slowly burning down the eastern face of Webbs Ridge toward C3. If the winds were to suddenly swing to the SSW due to channelling up the valley, then the northern flank would become a head-fire and burn up the valley in a direction almost perpendicular to the ambient winds. Once the fire burnt up out of the valley it would again experience westerly winds but would now have a much broader fire front due to the lateral spread caused by the up-valley channelling. It is of interest to note that the 1994 South Canyon fire in Colorado, which killed fourteen fire-fighters, behaved in a way that is consistent with that just described. In this incident a fire burning at the bottom of a north–south oriented canyon (known as the West Drainage) under the influence of westerly winds, rapidly spread in a northerly direction up the canyon before burning up the west-facing slopes and entrapping the fire-fighters. Witnesses reported southerly winds in the West

Drainage of 30–55 km h<sup>-1</sup> and westerly winds blowing across the ridges at 70 km h<sup>-1</sup> at the same time (Butler et al., 1998).

## 6. Conclusions

A probabilistic analysis of terrain-induced winds has been presented using measured data from a steep slope and an incised valley. The analysis focused on the structure of joint wind direction distributions for pairs of locations; one relating to the ambient wind direction and one relating to the terrain-modified wind at a point in the landscape. A clear majority of the joint distributions exhibited a modal structure, indicating distinct preferences for certain regions of the toroidal state space. Analysis of the timing of conditions corresponding to specific modes provided strong evidence for the existence of several different processes. These processes included thermally-driven upslope winds during the day and complementary downslope winds during the night-time, broader scale diurnal valley winds (up Flea Creek, for example), forced channelling along valleys and lee-slope eddies.

Another possible explanation for the differences in wind at different locations is atmospheric stability. This would especially apply during inversions when a low weather station in a valley or on a slope might be under the inversion and the ridge-top station is above it. This would effectively decouple the winds at the two stations. However, as it was not possible to make detailed stability measurements, this possibility was not considered in the study.

As the threshold wind speeds were increased, different modes responded in different ways. In particular, modes corresponding to processes such as channelling and lee-slope eddies were more dominant for higher wind speeds. This is not surprising since when the winds are strong, dynamic effects would tend to overpower the weaker thermal effects.

The similarity of the results for transect A and transect B suggest that they could be extrapolated with reasonable accuracy to other steep slopes that are aligned almost perpendicular to the main winds, particularly in regions that experience similar bimodal ambient wind fields. At the least, the results should cause fire managers to view lee-slopes, and the regions downwind, with caution, particularly when the ambient winds are over 8 ms<sup>-1</sup> (approx. 30 km h<sup>-1</sup>).

The analyses revealed the distinctly stochastic nature of the wind direction data. Given a fixed ambient wind direction, and without knowing the specific characteristics of the surrounding atmosphere, it does not seem possible to uniquely specify a corresponding terrain-modified wind direction with complete certainty. This suggests that a more probabilistic approach to the problem is appropriate; rather than specifying a wind direction, it should be sampled from the relevant distribution. Moreover, the results cast doubt upon the utility of deterministic methods that only employ wind speed and direction as inputs to estimate terrain-modified wind fields in rugged terrain. In particular it was shown that kinematic methods could be in error more than 75% of the time when applied to steep lee-slopes.

The majority of the modes we have observed in the joint wind distributions are located around specific points on the  $S^1 \times S^1$  torus (for example, (E, W)). In a dynamical systems sense, these points could perhaps be interpreted as attractors for the local meteorology. Investigating a suitable low dimensional system to verify this would be an interesting extension of the present work, but is beyond the scope of this paper.

## Acknowledgements

This work could not have been undertaken without the efforts of the staff of the Mechanical and Electrical Workshops in the School

of Physical, Environmental and Mathematical Sciences, University of New South Wales at the Australian Defence Force Academy. In particular, the authors gratefully acknowledge the contributions of Ray Lawton, Hans Lawatsch and Colin Symons who facilitated the modification of the PAWS units. The authors are also indebted to the staff of NSW National Parks and Wildlife Service and ACT Parks, Conservation and Lands. In particular, we would like to thank Susannah Power, Julie Crawford Lynn McCoustra and Joel Patterson. The authors would also like to thank Stephen Wilkes, Ian Knight, Terese Richardson, Steve Forbes, Alan Walker, Paul McKie, Tom Jovanovic and Peter Scott for their assistance with deploying the weather stations or with other field-work related activities. The authors appreciate the efforts of the three anonymous reviewers whose comments aided in clarifying many points in the paper and broadening its scope. This work was undertaken as part of the Bushfire CRC's HighFire Risk project. The support of the Bushfire CRC is acknowledged.

## References

- Alm, L.K., Nygaard, T.A., 1995. Flow over complex terrain estimated by a general purpose Navier-Stokes solver. *Modelling, Identification and Control* 16, 169–176.
- Barry, R.G., 1992. *Mountain Weather and Climate*, second ed. Routledge, New York.
- Beer, T., 1991. Bushfire rate of spread forecasting: deterministic and statistical approaches to fire modelling. *Journal of Forecasting* 10, 301–317.
- Blumen, W. (Ed.), 1990. *Atmospheric Processes over Complex Terrain*. Meteorological Monographs 23, No. 45. American Meteorological Society, Boston.
- Bowen, A.J., 2003. Modelling of strong wind flows over complex terrain at small geometric scales. *Journal of Wind Engineering and Industrial Aerodynamics* 91, 1859–1871.
- Bradstock, R., Price, O., 2010. Fire Severity Patterns in the Victorian Fires of February 7th 2009: Influences of Weather, Terrain and Land Use History. Report to the 2009 Victorian Bushfires Royal Commission. [www.royalcommission.vic.gov.au](http://www.royalcommission.vic.gov.au).
- Butler, B.W., Bartlette, R.A., BradshawCohen, J.D., Andrews, P., Putnam, T., 1998. Fire Behaviour Associated with the 1994 South Canyon Fire on Storm King Mountain, Colorado. Research Paper RMRMS-RP-9. USDA Forest Service, Rocky Mountain Research Station, Ogden, UT.
- Butler, B.W., Finney, M.A., Bradshaw, L.S., Forthofer, J.M., McHugh, C., Stratton, R., Jimenez, D., 2006a. WindWizard: a new tool for fire management decision support. In: Conference Proceedings: Fuels Management – How to Measure Success, March 28–30, 2006. Rocky Mountain Research Station, U.S. Department of Agriculture, Portland, OR Forest Service Proceedings RMRS-P-41.
- Butler, B.W., Forthofer, J.M., Finney, M.A., McHugh, C., Stratton, R., Bradshaw, L.S., 2006b. The impact of high resolution wind field simulations on the accuracy of fire growth predictions. In: Viegas, D.X. (Ed.), Proceedings of the 5th International Conference on Forest Fire Research, 27–30 November 2006 Figueira da Foz, Portugal.
- Byron-Scott, R.A.D., 1990. The effects of ridge-top and lee-slope fires upon rotor motions in the lee of a steep ridge. *Mathematical and Computer Modelling* 13 (12), 103–112.
- Chandler, C., Cheney, P., Thomas, P., Trabaud, L., Williams, D., 1983. *Fire in Forestry*. In: *Forest Fire Behaviour and Effects*, vol. 1. John Wiley and Sons, New York.
- Coen, J.L., 2005. Simulation of the Big Elk Fire using coupled atmosphere-fire modeling. *Journal of Wildland Fire* 14, 49–59.
- Davis, C.G., Bunker, S.S., Mutschlecner, J.P., 1984. Atmospheric transport model for complex terrain. *Journal of Climate and Applied Meteorology* 23, 235–238.
- Doran, J.C., Whiteman, C.D., 1992. The coupling of synoptic and valley winds in the Tennessee valley. In: Proceedings of the 6th Conference on Mountain Meteorology. American Meteorological Society, Boston.
- Eckman, R.M., Dobosy, R.J., Shankar Rao, K., 1992. Spatial variability of the wind over moderately complex terrain. In: Proceedings of the 6th Conference on Mountain Meteorology. American Meteorological Society, Boston.
- Fiedler, F., 1983. Einige Charakteristika der Strömungen im Oberrheingraben. *Wissenschaftliche Berichte des Meteorologischen Instituts der Universität Karlsruhe* 4, 113–123.
- Forthofer, J.M., Butler, B.W., Shannon, K.S., Finney, M.A., Bradshaw, L.S., Stratton, R., 2003. Predicting surface winds in complex terrain for use in fire spread models. In: Proceedings of the Fifth Symposium on Fire and Forest Meteorology and Second Wildland Fire Ecology and Fire Management Congress, November 16–20, 2003. American Meteorological Society, Orlando, FL.
- Forthofer, J.M., 2007. Modeling Wind in Complex Terrain for Use in Fire Spread Prediction. Master's Thesis. Colorado State University, Fort Collins, CO.
- Forthofer, J.M., Butler, B.W., March 26–30, 2007. Differences in simulated fire spread over Askervein hill using two advanced wind models and a traditional uniform wind field. In: Conference proceedings: The Fire Environment – Innovations, Management, and Policy, March 26–30, 2007. Rocky Mountain Research Station, U.S. Department of Agriculture, Destin, FL Forest Service Proceedings RMRS-P-46.
- Grant, A.L.M., Mason, P.J., 1990. Observations of boundary-layer structure over complex terrain. *Quarterly Journal of the Royal Meteorological Society* 116, 159–186.

- Hennessey, K.J., Whetton, P.H., Smith, I.N., Bathols, J.M., Hutchinson, M.F., Sharples, J.J., 2008. Climate change effects on snow conditions in mainland Australia and adaptation at ski resorts through snowmaking. *Climate Research* 35 (3), 255–270.
- Holtslag, A.A.M., 1984. Estimates of diabatic wind speed profiles from near-surface weather observations. *Boundary-Layer Meteorology* 29, 225–250.
- Hunt, J.C.R., Snyder, W.H., 1980. Experiments on stably and neutrally stratified flow over a three-dimensional hill. *Journal of Fluid Mechanics* 96, 671–704.
- Hutchinson, M.F., Bischof, R.J., 1983. A new method for estimating the spatial distribution of mean seasonal and annual rainfall applied to the Hunter Valley, New South Wales. *Australian Meteorological Magazine* 31, 179–184.
- Hutchinson, M.F., 1995a. Stochastic space-time weather models from ground-based data. *Agricultural and Forest Meteorology* 73, 237–264.
- Hutchinson, M.F., 1995b. Interpolation of mean precipitation using thin-plate smoothing splines. *International Journal of Geographic Information Systems* 9, 385–403.
- Hutchinson, M.F., 1998. Interpolation of rainfall data with thin-plate smoothing splines II: analysis of topographic dependence. *Journal of Geographic Information and Decision Analysis* 2 (2), 168–185.
- Hutchinson, M.F., 2003. ANUSPLIN Version 4.3. Centre for Resource and Environmental Studies. Australian National University. <http://cres.anu.edu.au/outputs/anusplin.html>.
- Jackson, P.S., Hunt, J.C.R., 1975. Turbulent wind flow over a low hill. *Quarterly Journal of the Royal Meteorological Society* 101, 929–955.
- Kim, H.G., Patel, V.C., Lee, C.M., 2000. Numerical simulation of wind flow over hilly terrain. *Journal of Wind Engineering and Industrial Aerodynamics* 87, 45–60.
- Kim, S.-E., Boysan, F., 1999. Application of CFD to environmental flows. *Journal of Wind Engineering and Industrial Aerodynamics* 81, 145–158.
- Kossmann, M., Sturman, A., Zavar-Reza, P., 2001. Atmospheric influences on bushfire propagation and smoke dispersion over complex terrain. In: *Proceedings of the Australasian Bushfire Conference*, 3–6 July 2001, Christchurch, New Zealand.
- Kossmann, M., Sturman, A.P., 17–21 June 2002. Dynamic airflow channelling effects in bent valleys. In: *Proceedings of the 10th Conference on Mountain Meteorology*. American Meteorological Society, Park City, UT.
- Kossmann, M., Sturman, A.P., 2003. Pressure-driven channelling effects in bent valleys. *Journal of Applied Meteorology* 42 (1), 151–158.
- Lee, J.T., Barr, S., Snyder, W.H., Lawson Jr., R.E., 9–12 November 1981. Wind tunnel studies of flow channelling in valleys. In: *Proceedings of the 2nd Conference on Mountain Meteorology*. American Meteorological Society, Steamboat Springs, CO.
- Lewis, H.W., Mobbs, S.D., Lehning, M., 2008. Observations of cross-ridge flows across steep terrain. *Quarterly Journal of the Royal Meteorological Society* 134, 801–816.
- Linn, R.R., 1997. Transport Model for Prediction of Wildfire Behaviour. Scientific Report LA13334-T. Los Alamos National Laboratory, Los Alamos, NM.
- Linn, R.R., Winterkamp, J.L., Edminster, C., Colman, J.J., Smith, W.S., 2007. Coupled influences of topography and wind on wildland fire behaviour. *International Journal of Wildland Fire* 16, 183–195.
- Lopes, A.M.G., 2003. WindStation – A software for the simulation of atmospheric flows over complex topography. *Environmental Modelling and Software* 18, 81–96.
- Mason, P.J., Sykes, R.I., 1979. Flow over an isolated hill of moderate slope. *Quarterly Journal of the Royal Meteorological Society* 105, 383–395.
- McCutchan, M.H., 1983. Comparing temperature and humidity on a mountain slope and in the free air nearby. *Monthly Weather Review* 111, 836–845.
- McCutchan, M.H., Fox, D.G., 1986. Effect of elevation and aspect on wind, temperature and humidity. *Journal of Climate and Applied Meteorology* 25, 1996–2013.
- McRae, R., 1997. Considerations on operational wildfire spread modelling. In: *Proceedings, Bushfire 1997*. Australasian Bushfire Conference, July 1997, Darwin.
- McRae, R., 2004. The breath of the dragon – observations of the January 2003 ACT bushfires. In: *Proceedings, Bushfire 2004*. South Australian Department of Environment and Heritage, Adelaide.
- McRae, R., Weber, R.O., Sharples, J.J., June 2006. Lessons from the 2003 fires – advancing bushfire risk management in the high country. In: *Proceedings, Bushfire 2006*, Brisbane.
- Mills, G.A., 2006. On the subsynoptic-scale meteorology of two extreme fire weather days during the Eastern Australian fire of January 2003. *Australian Meteorological Magazine* 54, 265–290.
- Mills, G.A., 2007. On easterly changes over elevated terrain in Australia's southeast. *Australian Meteorological Magazine* 56, 177–190.
- Moussiopoulos, N., Flassak, T., 1986. Two vectorized algorithms for the effective calculations of mass-consistent flow fields. *Journal of Applied Meteorology* 25, 847–857.
- Nairn, G., 2003. A Nation Charred: Inquiry into the Recent Australian Bushfires. The Parliament of the Commonwealth of Australia, Canberra.
- Ross, D.G., Smith, I.N., Manins, P.C., Fox, D.G., 1988. Diagnostic wind field modeling for complex terrain: model development and testing. *Journal of Applied Meteorology* 27, 785–796.
- Scorer, R.S., 1955. Theory of airflow over mountains: IV – Separation of flow from the surface. *Quarterly Journal of the Royal Meteorological Society* 81, 340–350.
- Sharples, J.J., Hutchinson, M.F., 2003. The horizontal scale of topographic dependence of monthly Australian precipitation. In: Post, D.A. (Ed.), *Proceedings of the International Congress on Modelling and Simulation 2003*, vol. 1, pp. 130–135.
- Sharples, J.J., Hutchinson, M.F., 12–15 December 2005. Spatio-temporal analysis of climatic data using additive regression splines. In: Zenger, A., Argent, R.M. (Eds.), *Advances and Applications for Management and Decision Making*. Proceedings of the International Congress on Modelling and Simulation Melbourne, Australia.
- Sharples, J.J., Hutchinson, M.F., Jellett, D.R., 2005. The horizontal scale of elevation dependence of monthly Australian precipitation. *Journal of Applied Meteorology* 44 (12), 1850–1866.
- Sharples, J.J., 2009. An overview of mountain meteorological effects relevant to fire behaviour and bushfire risk. *International Journal of Wildland Fire* 18, 737–754.
- Sherman, C.A., 1978. A mass-consistent model for wind fields over complex terrain. *Journal of Applied Meteorology* 17, 312–319.
- Smedman, A.-S., Bergström, H., Högström, U., 1996. Measured and modelled local wind fields over a frozen lake in a mountainous area. *Contributions to Atmospheric Physics* 69, 501–516.
- Sturman, A.P., 1987. Thermal influences on airflow in mountainous terrain. *Progress in Physical Geography* 11, 183–206.
- Tampieri, F., 1987. Separation features of boundary-layer flow over valleys. *Boundary-Layer Meteorology* 40, 195–307.
- Taylor, P.A., Mason, P.J., Bradley, E.F., 1987. Boundary-layer flow over low hills. *Boundary-Layer Meteorology* 39, 107–132.
- Taylor, J.R., Kossmann, M., Low, D.J., Zavar-Reza, P., 2005. Summertime easterly surges in southeastern Australia: a case study of thermally forced flow. *Australian Meteorological Magazine* 54, 213–223.
- Van Ulden, A.P., Holtslag, A.A.M., 1985. Estimation of atmospheric boundary layer parameters for diffusion applications. *Journal of Climate and Applied Meteorology* 24, 1196–1207.
- Wahba, G., 1990. Spline models for Observational data. CBMS-NSF Regional Conference Series in Applied Mathematics, SIAM, Philadelphia.
- Weber, R.O., Kauffmann, P., 1998. Relationship of synoptic winds and complex terrain flows during the MISTRAL field experiment. *Journal of Applied Meteorology* 37, 1486–1496.
- Whiteman, C.D., 1990. Observations of thermally developed wind systems in mountainous terrain. In: Blumen, W. (Ed.), *Atmospheric Processes over Complex Terrain*. Meteorological Monographs 23, No. 45. American Meteorological Society, Boston, pp. 5–42.
- Whiteman, C.D., Doran, J.C., 1993. The relationship between overlying synoptic-scale flows and winds within a valley. *Journal of Applied Meteorology* 32, 1669–1682.
- Whiteman, C.D., 2000. *Mountain Meteorology Fundamentals and Applications*. Oxford University Press, New York.
- Winterkamp, J.L., Linn, R.R., Colman, J.J., Smith, W.S., Edminster, C.B., Weise, D.R., 2006. Interaction between wildfires, atmosphere and topography. In: Viegas, D. X. (Ed.), *Proceedings of the 5th International Conference on Forest Fire Research*, 27–30 November 2006, Figueira da Foz, Portugal.
- Wippermann, F., Gross, G., 1981. On the constriction of orographically influenced wind roses for given distributions of the large-scale wind. *Contributions to Atmospheric Physics* 54, 492–501.
- Wippermann, F., 1984. Air flow over and in broad valleys: channelling and counter-current. *Contributions to Atmospheric Physics* 57, 92–105.
- Wood, N., Mason, P., 1993. The pressure force induced by neutral, turbulent flow over hills. *Quarterly Journal of the Royal Meteorological Society* 119, 1233–1267.
- Wood, N., 1995. The onset of separation in neutral, turbulent flow over hills. *Boundary-Layer Meteorology* 76, 137–164.
- Wood, N., 2000. Wind flow over complex terrain: a historical perspective and the prospect for large-eddy modelling. *Boundary-Layer Meteorology* 96, 11–32.